An Aurora kinase A-BOD1L1-PP2A B56 Axis promotes chromosome segregation fidelity

Thomas J. Kucharski[1], Irma M. Vlasac[2], Martin R. Higgs[3], Brock C. Christensen[2,4,5,6] and Duane A. Compton[1,6*]

1) Department of Biochemistry and Cell Biology, Geisel School of Medicine at Dartmouth,

2) Department of Epidemiology, Geisel School of Medicine at Dartmouth

3) Institute of Cancer and Genomic Sciences, University of Birmingham, Birmingham, B15 2TT, UK

4) Department of Molecular and Systems Biology, Geisel School of Medicine at Dartmouth

5) Department of Community and Family Medicine, Geisel School of Medicine at Dartmouth

6) Dartmouth Cancer Center, Geisel School of Medicine at Dartmouth, Lebanon, NH

*Corresponding author

Keywords: kinetochore, microtubule, mitosis, phosphorylation, Aurora, phosphatase

Correspondence address:
Department of Biochemistry and Cell Biology
Geisel School of Medicine at Dartmouth
WTRB Level 6
1 Medical Center Drive
Lebanon, N.H. 03756
USA
603-650-1190 (phone)
603-650-1128 (FAX)
duane.a.compton@dartmouth.edu
geiselmed.dartmouth.edu/compton/

Summary

Cancer cells are often aneuploid and frequently display elevated rates of chromosome mis-segregation in a phenomenon called chromosomal instability (CIN). CIN is commonly caused by hyperstable kinetochore-microtubule (K-MT) attachments that reduces the efficiency of correction of erroneous K-MT attachments. We recently showed that UMK57, a chemical agonist of MCAK (alias KIF2C), improves chromosome segregation fidelity in CIN cancer cells but that cells rapidly develop resistance to UMK57. To determine the mechanism of resistance we performed unbiased proteomic screens which revealed increased phosphorylation in cells adapted to UMK57 at two Aurora kinase A phosphoacceptor sites on BOD1L1 (alias FAM44A). BOD1L1 depletion or Aurora kinase A inhibition eliminated resistance to UMK57 in CIN cancer cells. BOD1L1 localizes to spindles/kinetochores during mitosis, interacts with the PP2A phosphatase, and regulates phosphorylation levels of kinetochore proteins, chromosome alignment, mitotic progression, and fidelity. Moreover, the *BOD1L1* gene is mutated in a subset of human cancers, and *BOD1L1* depletion reduces cell growth in combination with low doses of taxol or Aurora kinase A inhibitor. Thus, an Aurora kinase A -BOD1L1-PP2A axis promotes faithful chromosome segregation during mitosis.

46 **Introduction**

47 Faithful chromosome segregation during cell division relies on proper bioriented
48 attachment of kinetochores to spindle microtubules. Errors in kinetochore-microtubule (k-MT)
49 attachment arise frequently during early phases of mitosis and the persistence of these errors is a
50 common cause of the elevated rate of chromosome mis-segregation resulting in chromosomal
51 instability (CIN) and aneuploidy in solid tumors [1–5]. We previously demonstrated that strategies
52 that destabilize k-MT attachments promote faithful chromosome segregation in CIN cancer cells
53 by increasing the correction rate of k-MT attachment errors. Specifically, overexpression of
54 either MCAK (alias KIFC) or KIF2B microtubule depolymerases suppressed chromosome mis-
55 segregation in a variety of CIN cancer cell lines[5–8]. These data demonstrate the potential of
56 suppressing CIN as a strategy for cancer treatment.

57 To pursue this strategy, we recently characterized a cell-permeable small molecule
58 agonist of MCAK activity called UMK57. MCAK plays a key role at centromeres/kinetochores
59 by driving microtubule detachment to increase k-MT turnover to facilitate error correction prior
60 to anaphase[9,10]. At moderate dosage (100 nM), UMK57 increases the rate of k-MT detachment
61 and therefore decreases the rate of chromosome mis-segregation in anaphase. Surprisingly, high
62 rates of chromosome mis-segregation returned to CIN cancer cells after only ~72 hours of
63 treatment with UMK57. This resistance arose within the entire cell population, did not depend on
64 the activity of drug efflux pumps, changes in the level or localization of MCAK, or changes to
65 overall spindle morphology, and data demonstrated that MCAK activity continued to be
66 activated by UMK57 in treated cells. Thus, this represents adaptive resistance (as opposed to
67 acquired resistance which relies on the emergence of rare genetic variants) to UMK57 whereby
68 changes to cell signaling pathways bypass increased MCAK activity.

69 To determine the mechanisms by which CIN cancer cells develop resistance to UMK57,
70 we performed unbiased proteomic screens using mass spectrometry to identify changes in total
71 protein and protein phosphorylation levels between acutely treated and adapted cells in mitosis.
72 These screens revealed changes in phosphorylation of two Aurora kinase A sites in the C-
73 terminus of the large nuclear protein BOD1L1. Subsequent studies revealed that both Aurora
74 kinase A activity and BOD1L1 expression are required for cellular resistance to prolonged
75 UMK57 treatment. Moreover, BOD1L1 localizes to the mitotic spindle and kinetochores,
76 interacts with the Protein Phosphatase 2 (PP2A) complex and is required for setting correct
77 levels of kinetochore phosphorylation to support faithful chromosome segregation. Therefore,
78 cells rely on an Aurora kinase A-BOD1L1-PP2A axis to maintain proper k-MT attachment
79 stability for faithful chromosome segregation and utilize this axis to alter kinetochore
80 phosphorylation as a mechanism to adapt to persistent k-MT destabilization. Importantly,
81 BOD1L1 mutation is associated with improved prognosis in uterine endometrial cancer.
82 Accordingly, we show that loss of BOD1L1 expression reduces cellular fitness of cancer cell
83 lines in culture and induces catastrophic levels of chromosome mis-segregation in combination
84 with taxol and Aurora kinase A inhibitor.
85

86 **Results**

87 Proteomic analysis of UMK57 resistance in mitotic cells

88 To investigate the cellular mechanisms promoting resistance to UMK57, we developed
89 conditions for proteomic screens in mitotic cells (Figure 1A). We utilized SW620 (lymph node
90 metastasis of colon cancer) cells for this purpose because they are CIN and they undergo
91 adaptive resistance to UMK57[11]. Specifically, SW620 cells naïve to UMK57 display lagging
92 chromosomes in 34% of anaphases, on average. The rate of lagging chromosomes in anaphase
93 decreases to 25% upon treatment with 100nM UMK57 for 1 hour, and rebounds to 37%
94 following 72 hours continuous treatment (Figure 1B). SW620 cells also display reduced
95 phosphorylation of MCAK pS95 and Aurora kinase B pT232 following 72 hours continuous
96 treatment with UMK57 consistent with our previous findings indicating that changes in
97 centromere/kinetochore phosphorylation levels correlated with the adaptive resistance response
98 (Figure S1A-D). Therefore, SW620 cells likely adapt to UMK57 by altering signaling networks
99 leading to changes in the phosphorylation of specific kinetochore proteins, as suggested
100 previously[11].

101 For proteomic analysis, we first treated SW620 cells with 100nM UMK57 for 72 hours to
102 represent the adapted condition. A parallel set of cells was treated with DMSO for 72 hours. The
103 cells were then synchronized by thymidine-nocodazole (still in the presence of DMSO/UMK57)
104 followed by 1 hour treatment of the DMSO population with 100nM UMK57 immediately prior
105 to harvest to represent the acutely treated condition. Mitotic cells were harvested by shake-off
106 and compared for differences in total protein level and protein phosphorylation level using by
107 mass spectrometry (Figure 1A).

108 For comparison of total protein levels, we obtained data for 6966 proteins based on 7,704
109 unique and 150,981 total peptides (Figure 1C). Among these, protein levels between the two cell
110 populations varied from +1.725 to 0.41-fold change with 6,813 proteins (97.7%) varying
111 between the two cell populations within +1.2 and 0.8-fold-change. Protein levels skewed towards
112 increased levels in one biological replicate resulting in a skewed overall distribution (Figure S1E,
113 supplemental table 1). Among the proteins identified, the levels of Sgo2 were significantly
114 increased (#38, +1.30-fold, $p = 0.0037$, 6 peptides) in adapted cells. Sgo2 is an interesting
115 candidate for involvement in UMK57 adaptation as it is extensively implicated in setting
116 kinetochore phosphorylation levels[12,13]. However, independent validation of a change in Sgo2
117 protein level by immunoblot was inconclusive (Figure S2F). The catalytic subunit of PP2A
118 (PPP2CB) appeared to be decreased in protein level in adapted cells, although that was based on
119 a single peptide and so was discarded (supplemental table 1). Thus, total protein levels in mitotic
120 SW620 cells that have adapted to UMK57 change very little, and generally within a narrow
121 range, relative to mitotic SW620 cells that are acutely treated with UMK57.
122 We next examined the phospho-proteomic changes in mitotic SW620 cells that have
123 adapted to UMK57 versus cells that are acutely treated. We obtained data from 47,550 unique
124 peptides from 122,241 total peptides. Of these, 31,563 sites were quantified, and 23,155 sites
125 were both quantified and localized (Figure 1C, supplemental table 2). Among these, phospho-
126 peptide levels between the two cell populations varied from 2.98 to 0.27-fold change with 19,973
127 (86.2%) varying between the two cell populations within 1.2 to 0.8-fold-change. 6,378 phospho-
128 peptides displayed an increased abundance in UMK57 adapted cells and 16,777 peptides showed
129 decreased abundance.

130 We performed Gene ontology analysis on the group of proteins that displayed significant
131 changes in peptide phosphorylation ($p < 0.1$). We included both proteins showing increases or
132 decreases in protein phosphorylation to capture changes caused by altered kinase or phosphatase
133 activity. This analysis revealed significant over-representation of proteins involved in mitotic
134 processes including chromosome condensation, centromere/chromosome localization, and
135 microtubule polymerization and de-polymerization, consistent with an adaptive resistance to
136 UMK57 altering mitotic processes including microtubule dynamics (Figure 1D). STRING
137 protein-protein interaction network analysis of the top and bottom 100 proteins displaying the
138 largest, significant changes in peptide phosphorylation revealed a cluster of proteins involved in
139 mitosis. Of these, proteins with peptides displaying significantly increased levels of
140 phosphorylation in adapted cells relative to acutely treated cells include Numa, 53BP1, Ska3,
141 INCENP and BOD1L1 (Alias FAM44A). Proteins with peptides displaying significantly
142 decreased levels of phosphorylation in adapted cells relative to acutely treated cells included
143 Knl1, Numa, Hec1, NUSAP, INCENP and TPX2 (Figure 1F, supplemental table 2). Thus, our
144 dataset contains proteins whose phosphoregulation might plausibly mediate adaptation to
145 UMK57.
146 Analysis of the amino acid sequences of the potential phosphoacceptor sites identified in
147 the screen with significant changes in phosphorylation level ($p<0.1$) shows over-representation
148 of the canonical Cdk phosphorylation site motif (S/TPxxK) and possibly Aurora kinase motifs
149 (R/KR/KxS/T) (Figure 1E). We explored if there was enrichment of Aurora substrates in our
150 dataset utilizing a previous screen that identified many Aurora-dependent phosphoacceptor sites
151 in mitosis[14] and that categorized peptides as being selectively phosphorylated by either Aurora
152 kinase A or Aurora kinase B using selective chemical inhibitors of those kinases. This analysis

153 revealed a 10.1- and 12.6-fold over-representation of Aurora kinase A substrates and Aurora
154 kinase B substrates, respectively, among the population of phosphoacceptor sites identified in
155 our dataset, although many phosphoacceptor sites could be phosphorylated by both kinases
156 (Figure 1G).

157 Among all proteins that displayed changes in phosphorylation level in adapted cells
158 relative to acutely treated cells, BOD1L1 demonstrated the most significant change. 32 different
159 BOD1L1 phospho-peptides were detected in the phospho-proteomic screen, of which 3 showed
160 statistically significant positive changes, and two statistically significant negative changes.
161 BOD1L1 (FAM44A) is closely related to Bod1 (FAM44B) and Bod1L2 (FAM44C) but contains
162 a short proline rich n-terminal extension, and a long, c-terminal extension (Figure 1H). Of note,
163 one BOD1L1 peptide was doubly phosphorylated on T2956 and S2958 and displayed a
164 significant increase (1.3-fold; $p = 0.06$) in phosphorylation in adapted cells relative to acutely
165 treated cells. Another peptide was also doubly phosphorylated and contains S2973 and S2986
166 and displayed a significant increase (2.3-fold; $p < 0.01$) in phosphorylation in adapted cells
167 relative to acutely treated cells. Another peptide was singly phosphorylated at S2986 and
168 displayed a significant increase (1.2-fold; $p = 0.07$) in phosphorylation in adapted cells relative to
169 acutely treated cells. Importantly, the total protein level of BOD1L1 did not change in adapted
170 cells relative to acutely treated cells (1.06-fold; $p = 0.26$; 15 peptides) (Figure 1F, supplemental
171 table 1) indicating that BOD1L1 undergoes net changes in phosphorylation status as cell adapt to
172 UMK57. The peptide containing S2954, T2956 and S2958 was previously identified in a
173 phospho-proteomic screen[14], and the conserved cluster of lysine and arginine residues proximal
174 to the phosphoacceptor sites suggest phosphorylation by Aurora kinases (figure 1I). Indeed,
175 previous proteomic analysis demonstrated that phosphorylation of this peptide is sensitive to an

176 Aurora kinase A inhibitor in a dose-dependent manner, and insensitive to an inhibitor of Aurora
177 kinase B (Figure S1H)[14]. Moreover, BOD1L1 was previously detected in an Aurora kinase A
178 proximity-ligation mapping experiment[15]. These data indicate that BOD1L1 is selectively
179 phosphorylated by Aurora kinase A as cells adapt to UMK57. Interestingly, BOD1L1 is
180 distinguished from other members of this gene family because neither Bod1 nor Bod1L2 contain
181 obvious Aurora kinase consensus sites and the phosphoacceptor sites identified here and in
182 previous proteomic screens are in the extended c-terminal domain that is unique to BOD1L1, in
183 agreement with the fact that BOD1L1 is functionally distinct from BOD1 during DNA repair[16].
184

185 <u>BOD1L1 and Aurora kinase A are required for adaptation to UMK57</u>

186 To determine if BOD1L1 is functionally required for adaptive resistance to UMK57 in
187 CIN cancer cells, we used two independent shRNA sequences to knockdown BOD1L1
188 expression and selected cells for shRNA expression using puromycin treatment. We confirmed a
189 durable knockdown of BOD1L1 over several days in cells expressing BOD1L1 shRNA
190 compared to cells expressing control shRNA using BodlL1-specific antibodies on immunoblot
191 and through indirect immunofluorescence. (Figure S2A, S2B).

192 Next, we tested if BOD1L1 is required for cells to adapt to UMK57. We transfected cells
193 with BOD1L1-specific shRNA or control shRNA expressing plasmids, selected for puromycin
194 resistance, added UMK57 for short or prolonged periods and then measured the frequency of
195 lagging chromosomes during mitosis. As expected in cells transfected with control shRNA, acute
196 treatment with UMK57 reduces the frequency of lagging chromosomes in anaphase and high
197 lagging chromosome rates return upon prolonged treatment with UMK57. Cells transfected with
198 either of two distinct BOD1L1 shRNA's display elevated rates of lagging chromosomes in

199 anaphase compared to cells transfected with control shRNA. BOD1L1-deficient cells respond to
200 acute treatment with UMK57 and show significantly fewer anaphase cells with lagging
201 chromosomes. The effect of UMK57 on BOD1L1-deficient cells is durable because cells retain
202 significantly reduced lagging chromosome rates compared to DMSO-treated cells (Figure 2A,
203 2B). Therefore, BOD1L1 expression is required for adaptation to prolonged UMK57 treatment.
204 Since BOD1L1 is phosphorylated by Aurora kinase A in mitosis and there was a
205 significant increase in BOD1L1 phosphorylation during adaptation to prolonged UMK57
206 treatment, we also tested if Aurora kinase A activity is required for adaptation to UMK57. We
207 treated cells concurrently with a sublethal dose of Aurora kinase A inhibitor and UMK57 over 3
208 days and assessed the rates of lagging chromosomes. SW620 cells continued to proliferate in the
209 presence of Aurora kinase A inhibitor (Figure S2C), and cells treated with Aurora kinase A
210 inhibitor alone displayed elevated levels of lagging chromosomes compared to cells treated with
211 DMSO. Cells treated with Aurora kinase A inhibitor respond to acute treatment with UMK57
212 and display significantly fewer lagging chromosomes in anaphase relative to cells treated with
213 the Aurora kinase A inhibitor alone. The fraction of anaphase cells with lagging chromosomes
214 remained significantly reduced in cells with prolonged UMK57 treatment when Aurora kinase A
215 was inhibited demonstrating that Aurora kinase A is also required for adaptation to prolonged
216 UMK57 treatment (Figure 2C).
217 These and previous data[11] indicate that adaptation to prolonged UMK57 treatment likely
218 occurs through changes in kinetochore protein phosphorylation and that BOD1L1 may play a
219 role in regulating protein phosphorylation. Therefore, we tested if treatment of cells with a
220 modest dose of Okadaic acid[17], which inhibits PP2A and to a lesser extent PP1 phosphatases,
221 would alter the rate of lagging chromosomes in anaphase. Cells transfected with control shRNA

222 displayed a reduced frequency of lagging chromosomes in anaphase when treated with Okadaic
223 acid, suggesting that elevated protein phosphorylation can increase chromosome segregation
224 fidelity (Figure 2D). As expected, BOD1L1-deficient cells display elevated numbers of lagging
225 chromosomes in anaphase. Remarkably, cells transfected with shRNA against BOD1L1 and
226 treated with Okadaic acid had rates of lagging chromosomes in anaphase that were not different
227 from control shRNA/DMSO treated cells. Thus, Okadaic acid treatment effectively replaces
228 BOD1L1 function in mitosis as measured by chromosome segregation fidelity indicating that
229 BOD1L1 likely acts as a negative regulator of protein phosphatase activity and that the elevated
230 rate of lagging chromosomes in BOD1L1-deficient cells (Figure 2A) is due to reduced levels of
231 protein phosphorylation.

232 Since Aurora kinase A is required for adaptation to UMK57, we used cell biological
233 approaches to test if Aurora kinase A activity is altered in cells treated either acutely with or
234 adapted to UMK57. We measured the intensity of Aurora kinase A and pT288 Aurora kinase A,
235 a marker of Aurora kinase A activity in mitotic cells from an asynchronous culture. Whereas the
236 ratio of Aurora kinase A to pT288 Aurora kinase A remained unchanged in cells treated acutely
237 with or adapted to UMK57 compared to control cells (i.e., no change in phospho-occupancy), the
238 overall levels of both Aurora kinase A and pT288 Aurora kinase A on mitotic spindles strongly
239 increased in cells treated with UMK57 (Figure 3A, 3B). Since TPX2 directs Aurora kinase A to
240 the mitotic spindle[18], we quantified the levels of TPX2 and alpha tubulin in the mitotic spindle in
241 cells treated with UMK57. Similar to Aurora kinase A, this experiment revealed elevated levels
242 of TPX2 on the mitotic spindle in cells treated with UMK57 despite a decrease in overall levels
243 of spindle microtubule content in treated cells (Figure 3C, 3E). TACC3, another spindle-
244 associated protein, displayed spindle intensity that roughly mirrored the levels of spindle

245 microtubule content (Figure 3D, 3E) indicating that the quantity of Aurora kinase A and TPX2
246 on spindles selectively increased upon UMK57 treatment.
247
248 BOD1L1 regulates mitotic progression and mitotic fidelity
249 To date, the only role identified for BOD1L1 is in DNA repair[16,19,20]. BOD1L1 shares
250 extensive sequence similarity to Bod1 which has been shown to be involved in regulation of
251 mitotic activities including kinetochore protein phosphorylation by recruiting the PP2A-B56
252 phosphatase, regulating MCAK localization, and also to be important for chromosome
253 alignment[21–23]. Given the similarities between Bod1 and BOD1L1, and that BOD1L1-deficient
254 cells display increased rates of lagging chromosomes in anaphase and that BOD1L1 function in
255 mitotic fidelity can be rescued using protein phosphatase inhibitors, we focused our efforts on
256 understanding the contribution of BOD1L1 to mitotic processes and chromosome segregation
257 fidelity.
258 Using immunofluorescence microscopy we detected BOD1L1 at spindle poles, on
259 microtubules and at kinetochores of SW620 cells (Figure 4A, 4B). Line scans showed significant
260 overlap between BOD1L1 and Hec1 at kinetochores in prometaphase through anaphase.
261 Notably, BOD1L1 does not localize to all kinetochores, but rather to a subset, suggesting the
262 possibility of regulation of BOD1L1 localization. Since BOD1L1 localizes to the mitotic spindle,
263 we also examined if BOD1L1 co-localizes with Aurora kinase A. We found a large degree of co-
264 localization between Aurora kinase A and BOD1L1 at the spindle poles and along pole-proximal
265 microtubules (Figure 4C). BOD1L1 co-localized with Hec1 on kinetochores in cells treated with
266 either a low or high dose of nocodazole demonstrating that BOD1L1 does not require
267 microtubules for kinetochore localization (Figure S2D). BOD1L1 localization was also

268 unchanged by treatment of cells with Aurora kinase A or Aurora kinase B inhibitors
269 demonstrating that BOD1L1 kinetochore localization is Independent of these kinase activities
270 despite the problems in spindle structure and chromosome alignment caused by these inhibitors
271 (Figure S2E).

272 BOD1L1-deficient cells appear to have aberrant spindle structures and problems with
273 chromosome alignment. We quantified these phenotypes by measuring the proportion of cells in
274 each phase of mitosis as a percentage of all mitotic cells. BOD1L1-deficient early prometaphase
275 cells often had small spindles with kinetochores located close to the poles, whereas late
276 prometaphase cells had difficulties in chromosome alignment (Figure 5A, 5B), with many
277 chromosomes located proximal to the spindle poles. We also used time-lapse microscopy on
278 mCherry-H2B expressing SW620 cells to measure the time spent in mitosis with and without
279 BOD1L1. Control cells needed on average 57 minutes to transit mitosis from the onset of
280 chromosome condensation to anaphase. In contrast, BOD1L1-deficient cells spent on average
281 208.3 minutes (shRNA #1) and 120.6 minutes (shRNA #2) in mitosis. These changes in the
282 average time taken to complete mitosis overestimates the overall impact of mitotic delay in
283 BOD1L1-deficient cells because it is skewed by cells that either underwent slippage or death
284 following extended times in mitosis. Amongst cells that completed mitosis with anaphase, these
285 cells took an average of 137.5 (shRNA #1) and 100.0 minutes (shRNA #2) to transit mitosis
286 (Figure 5C, S3A). Thus, BOD1L1 is functionally required for efficient mitotic progression.

287 Next, we tested if BOD1L1 contributes to k-MT attachment stability. Following
288 transfection with control or BOD1L1-specific shRNA plasmids and puromycin selection, we
289 cold treated cells to eliminate non-k-MT from spindles and fixed and stained cells for tubulin and

290 ACA. The spindle microtubule intensity in BOD1L1-deficient cells was increased in both
291 prometaphase and metaphase relative to cells transfected with control shRNA (Figure 5D, E).
292
293 BOD1L1 interacts with the PP2A-B56 phosphatase and regulates kinetochore phosphorylation
294 To gain further insight into the role(s) of BOD1L1 in mitosis, we immunoprecipitated
295 BOD1L1 from mitotic cells to determine the identity of interacting proteins. We cross-linked
296 antibody to protein G beads and used them to immunoprecipitate BOD1L1 interacting proteins
297 from SW620 cells synchronized in mitosis through sequential treatment with thymidine and
298 nocodazole. The eluted proteins were then separated by SDS-PAGE gel, stained with Coomassie,
299 cut into fractions and analyzed by mass spectrometry (Figure 6A). This analysis revealed a high
300 affinity interaction with the MTORC2 signaling complex which regulates cellular pro-survival
301 and is typified by the presence of the Rictor protein subunit[24] as judged by the very high number
302 of detected peptides. Also, there were numerous mRNA translation initiation factor proteins, and
303 abundant peptides from the CCT chaperone complex. In addition, we detected several proteins
304 that participate in DNA repair, including SETD1A, RAD50, XRCC5, XRCC6, RIF1 and
305 MRE11, consistent with previous findings, and which serve as positive controls for the
306 specificity of our assay[19,20]. We also detected various core subunits of the Anaphase Promoting
307 Complex/Cyclosome, although we did not detect the co-activator proteins Cdh1 or Cdc20. Thus,
308 BOD1L1 may be an APC/C substrate or a regulator of APC/C activity. We also detected
309 numerous proteins with documented mitotic functions including Sgo2, CENPF, MCAK, Numa,
310 Aurora kinase A, and several components of the PP2A-B56 phosphatase complex including both
311 PPP2R1A and PPP2R1B regulatory subunits, the PPP2CA catalytic subunit, and the PPP2R5E
312 epsilon adaptor subunit (Figure 6B, Supplemental table 3). Therefore, like Bod1, BOD1L1

313 interacts with PP2A and may regulate PP2A activity or is itself regulated by PP2A. These
314 interacting proteins were independently validated by blotting for various proteins. We detected
315 the PP2A catalytic, regulatory and the delta, gamma, and epsilon adaptor subunits, but not the
316 beta subunit. We also detected CENPF, MCAK, Bub3, SMC1 and APC3 proteins in BOD1L1
317 immunoprecipitates (Figure 6C). These interactions were generally enriched when BOD1L1 was
318 immunoprecipitated from cells synchronized in mitosis, compared to asynchronous cells.

319 There are notable similarities and differences in the interactomes of Bod1 and
320 BOD1L1[23]. Like Bod1, BOD1L1 interacts with PP2A-B56, SMC1A, SMC3, SETD1A, Aurora
321 kinase A and Bub3. In contrast, Bod1 did not show interaction with the MTORC2 complex, but
322 does interact with Hec1, Knl1 and components of the fibrous corona including Zwint, ZW10 and
323 dynein. Hec1 is among the strongest interacting proteins with Bod1 but was not detected as an
324 interactor with BOD1L1 in our analysis despite the co-localization of BOD1L1 with Hec1 at
325 kinetochores at the resolution of immunofluorescence microscopy. To test directly if BOD1L1
326 kinetochore localization requires Hec1, we utilized HeLa cells with doxycycline inducible
327 CRISPR/Cas9 Hec1 genetic knockout[25], and compared the localization of Bod1 in the presence
328 and absence of Hec1. We did not detect a significant change in BOD1L1 localization indicating
329 that Hec1 is not required for BOD1L1 kinetochore localization (Figure S3B).

330 To determine which domain of BOD1L1 is responsible for interaction with the PP2A
331 complex, we performed a pull-down experiment using fragments of BOD1L1 fused to GST as
332 bait from lysates of mitotic SW620 cells. Surprisingly, despite the high degree of similarity
333 between the n-terminus of BOD1L1 and Bod1 and the fact that both Bod1 and BOD1L1 interact
334 with PP2A subunits, the region of BOD1L1 that bound to the PP2A complex most strongly was
335 the uncharacterized central domain from amino acid 500 to 2001. Additionally, the c-terminal F6

336 fragment also interacted with the PP2A B56 delta subunit (Figure 6D). In contrast, it is the n-
337 terminal F1-F2 Bod1-similar and C-terminal F6 regions that bind Rif1 in the context of the DNA
338 damage response[19].
339 These data indicate that BOD1L1 might regulate the PP2A-B56 complex during mitosis
340 to regulate mitotic fidelity. Therefore, we tested whether BOD1L1 regulates kinetochore protein
341 phosphorylation levels in a similar manner to Bod1. Using immunofluorescence, we quantified
342 the staining intensity for numerous phosphorylated proteins at kinetochores following depletion
343 of BOD1L1. We stained cells for Aurora kinase A pT288 (Aurora kinase A), Hec1 pS55 (Aurora
344 kinase A), Hec1 pT31 (Cdk1-Cyclin B1), Hec1 pS44 (Aurora kinase B), Dsn1 pS100 (Aurora
345 kinase B), Knl1 pMELT (Mps1), Aurora kinase B pT232 (Aurora kinase B) and MCAK pS95
346 (Aurora kinase B). We observed that the intensity of staining for Hec1 pS55, Hec1 pT31, Hec1
347 pS44, pDsn1 pS100, and Knl1 pMELT decreased in both prometaphase and metaphase and
348 Aurora kinase B pT232 levels decreased in prometaphase in BOD1L1-deficient cells. In contrast,
349 MCAK pS95 staining intensity increased in metaphase cells (Figure 7). Notably, we did not
350 detect a pattern of changes for Aurora kinase A pT288, indicating that total Aurora kinase A
351 activity levels are essentially unchanged in BOD1L1-deficient mitotic cells. These results
352 combined with previous data showing that phosphatase inhibitors can rescue lagging
353 chromosomes in BOD1L1-deficient mitotic cells demonstrate that BOD1L1 functions as a
354 negative regulator of protein phosphatase activity to support efficient mitotic progression.
355 Consistently, the loss of BOD1L1 affects phospho-substrates at kinetochores that are
356 phosphorylated by multiple distinct protein kinases.
357
358 *BOD1L1* gene is mutated in human cancers

359 Since aneuploidy is associated with cancer development and BOD1L1-deficiency
360 increases mitotic error rates, we examined whether BOD1L1 is mutated in human cancers. We
361 queried The Cancer Genome Atlas (TCGA) for cancers that have somatic alterations in the wild-
362 type sequence in *BOD1L1*. Among the 10,967 cancers that have been sequenced, 3.9% of
363 cancers show alterations in *BOD1L1* sequence, although the prevalence of *BOD1L1* alterations
364 was variable across cancer types. The five cancers with the highest percentage of *BOD1L1*
365 somatic alterations are uterine endometrial carcinoma (12.9%), lung adenocarcinoma (8.8%),
366 skin cutaneous melanoma (7.9%), stomach adenocarcinoma (7.7%) and lung squamous cell
367 carcinoma (6.6%). Because our data demonstrate that BOD1L1 is activated by Aurora kinase A
368 and functionally regulates PP2A activity, we also examined the TCGA for cancers that have
369 alterations in any of *BOD1L1*, *AURKA, TPX2, PPP2CA, PPP2CB, PPP2R1A, PPP2R1B,*
370 *PPP2R5A, PPP2R5B, PPP2R5C, PPP2R5D, PPP2R5E*. Surprisingly, 59.6% of uterine
371 carcinosarcoma and 43.9% of uterine endometrial cancers have alterations in one or more of
372 these genes, suggesting that genes in this biochemical pathway might be particularly relevant in
373 these cancer types (Figure S4A). We next tested associations of *BOD1L1* alteration with 5-year
374 overall survival adjusting for potential confounders in these patients. *BOD1L1* alteration was
375 significantly associated with improved 5-year survival in uterine cancer HR = 0.37 (95% CI:0.16
376 – 0.85). *BOD1L1* alteration was significantly associated with reduced 5-year survival in lung
377 adenocarcinoma HR = 1.66 (95% CI: 1.03-2.66) and in melanoma HR = 1.79 (95% CI: 1.07-
378 3.00). *BOD1L1* alteration did not demonstrate a significant association with patient survival in
379 stomach adenocarcinoma or lung squamous cell carcinoma (Figure 8B).
380 Given that BOD1L1 appears to function in a pathway consisting of Aurora kinase A-
381 BOD1L1-PP2A B56, we asked if individuals with mutations in *BOD1L1* also have co-occurring

382 mutations in either *AURKA* or its cofactor *TPX2* or in *PP2A* complex components. Using data
383 from the TCGA-PanCancer Atlas (n = 10,967), we observed that *BOD1L1* alterations were
384 exclusive of alterations to other *AURKA-BOD1L1- PP2A* gene pathway members. This was true
385 when testing *BOD1L1* alteration versus alteration to any other gene pathway member (Fisher's
386 exact P=1.3E-24), and *BOD1L1* alteration versus each of the eleven gene pathway members
387 independently (all Fisher's exact P<5.7E-08) (Figure S4B, S4C), suggesting that mutations in
388 multiple components of this pathway are not tolerated in cancers.

389 To understand how BOD1L1 inactivation affects cell proliferation and response to anti-
390 mitotic drugs including Aurora kinase A inhibitors or taxol, we compared the proliferation of
391 cells derived from various tumor types [U2OS (osteosarcoma), HCT116 (colorectal carcinoma),
392 SW620 (colorectal adenocarcinoma), HeLa (cervical adenocarcinoma) and HEC1 (uterine
393 endometrial adenocarcinoma)] following transfection with either control shRNA or BOD1L1-
394 specific shRNA. All of these cell lines express detectable BOD1L1, albeit at different levels, and
395 they all require BOD1L1 for mitotic fidelity because there was a significant increase in lagging
396 chromosome rates in all cell lines following shRNA-mediated depletion of BOD1L1. (Figure
397 S4D & S4E). All cell types tested have reduced proliferation following transfection with the
398 BOD1L1-specific shRNA compared to the control shRNA, although the magnitude of the
399 reduction varied between cell types. This variance was not proportional to the level of BOD1L1
400 expression (e.g. HEC1 and SW620 cells have comparable expression levels, but different
401 BOD1L1 sensitivities) (Figure 8C, 8D, S4D, S4G). The proliferation of these cells following
402 treatment with taxol and Aurora kinase A inhibitor also varied. Proliferation of HCT116 cells
403 was modestly reduced by depletion of BOD1L1, but profoundly suppressed by treatment with
404 either dose of either drug with or without BOD1L1. In contrast, there was a dose-dependent

405 reduction in proliferation of U2OS, HeLa, HEC1 and SW620 cells in response to each drug.
406 When combined with BOD1L1 deficiency, the lower dose of each drug caused a substantial
407 further reduction in cell proliferation in U2OS cells, while HeLa cells were less affected and
408 SW620 cells were not affected by the combination of BOD1L1 knockdown and taxol or Aurora
409 kinase A inhibitor (Figure 8C, 8D, S4G). In line with the differential toxicity that we observed,
410 U2OS cells with BOD1L1 knockdown formed micronuclei at a higher rate compared to control
411 cells, while in SW620 cells there was no difference in micronuclei formation between control
412 and BOD1L1 knockdown conditions (Figure S4F). Thus, the relative impact of BOD1L1 gene
413 alteration on patient cancer survival is variable which is mirrored by a variable impact on
414 proliferation of various cell types following BOD1L1 depletion.
415

416 **Discussion**

417 Using an unbiased proteomic screen, we have discovered a pathway that regulates mitotic
418 fidelity by controlling phosphatase activity directed at kinetochore substrates. In an unperturbed
419 mitosis, BOD1L1 binds and inhibits PP2A-B56, helping to maintain moderate levels of
420 phosphorylation of kinetochore substrates, thus decreasing k-MT attachment stability and
421 ultimately supporting mitotic progression and high chromosome segregation fidelity. We
422 envision a scenario that when CIN cancer cells are treated for prolonged periods with UMK57 to
423 destabilize k-MT attachments, the adaptation response involves an increase in recruitment of
424 Aurora kinase A to spindles through TPX2 which increases phosphorylation of BOD1L1 and
425 relieves the negative regulation of PP2A activity. Relief of this constraint on PP2A leads to
426 reduced phosphorylation of numerous kinetochore substrates at the k-MT interface which
427 restores hyperstable k-MT stability and resumes the CIN phenotype (Figure 8E). This
428 mechanism for adaptation to UMK57 is consistent with data showing that small changes in
429 kinetochore phosphorylation can cause large changes in chromosome segregation fidelity[26–28],
430 and that the mechanism of adaptation is independent of the continued functional impact of
431 UMK57 to activate MCAK[11]. Interestingly, it has been shown recently that cells adapt to
432 oncogenic RAS/MAPK signaling by becoming increasingly dependent on BubR1/PP2A. This is
433 because signaling through RAS/MAPK results in hyperactivity of mitotic kinases, reducing k-
434 MT stability and increasing dependence on BubR1/PP2A to maintain viable levels of
435 phosphorylation[29]. Thus, deregulation of phosphatase activity toward kinetochores substrates
436 appears to be a common cellular response to pathways that change mitotic fidelity.

437 Notably, despite sharing a conserved domain, BOD1L1 and Bod1 do not bind PP2A
438 through the same region. Our data show that BOD1L1 binds to PP2A with the middle of the

439 protein which is not part of a conserved domain with Bod1 (Figure 6D). Therefore, although the
440 PP2A regulating function of Bod1 and BOD1L1 is conserved[22], the mechanism of their
441 interaction with PP2A is not. In addition, BOD1L1 has gained the ability to regulate DNA repair
442 through binding Rif1 at the n-terminus[19] and shifted the PP2A binding region to a large middle
443 region of the protein plus the c-terminus. This genetic separation of DNA damage and PP2A
444 regulating functions might explain the long c-terminal extension present in BOD1L1 compared
445 to Bod1 and Bod1L2. Importantly, the phosphoacceptor sites on BOD1L1 that increase
446 phosphorylation during the adaptation response to UMK57 also reside in the c-terminal domain
447 of the protein and are not conserved with Bod1. Thus, the regulation of BOD1L1 by Aurora
448 kinase A phosphorylation is distinct from processes that regulate Bod1.

449 A prevailing model differentiating the functional roles of Aurora A and B kinases in
450 mitosis is that although they both use the same consensus motif to recognize substrates, their
451 impact is different because they are spatially separated, with Aurora kinase A residing at spindle
452 poles and on microtubules, and Aurora kinase B at centromeres. Although compelling, this
453 model continues to be refined based on recent findings that some or perhaps even most non-CDK
454 phosphorylation sites on Hec1 at kinetochores are phosphorylated by Aurora kinase A rather
455 than Aurora kinase B[27,30,31] and other data indicating that Aurora kinase B can fulfill its mitotic
456 function without being targeted to centromeres in some systems[32]. Compared to Aurora kinase B,
457 relatively little is known about how Aurora kinase A regulates k-MT attachments, although
458 recent studies indicate that Aurora kinase A might also localize to kinetochores and
459 phosphorylate substrates there or regulate kinetochore substrates on chromosomes proximal to
460 the spindle pole[30,31]. Our data demonstrates that Aurora kinase A also regulates kinetochore
461 substrate phosphorylation indirectly through regulation of BOD1L1 as a negative regulator of

462 PP2A, and that this role for Aurora kinase A is responsible for changes in k-MT attachment
463 stability induced by prolonged increase in MCAK activity caused by UMK57 treatment. In this
464 context, an intriguing possibility emerges whereby the Aurora kinase A – BOD1L1 – PP2A axis
465 identified in this work is activated by hypostable k-MT attachments (or hypostable spindle MTs
466 more broadly) and induces a compensating increase in k-MT stability. Conversely, Aurora kinase
467 B has a well-recognized role in decreasing k-MT stability. Together, overall k-MT stability (and
468 perhaps total spindle MT stability and/or density) would be established through a lower bound
469 regulated by Aurora kinase A activity and an upper bound regulated by Aurora kinase B activity.
470 In support of this idea, TPX2 may serve as a sensor of MT stability to marshal Aurora kinase A
471 as needed because TPX2 has been shown to sense and influence the conformational state of
472 microtubules[33] while promoting MT assembly by suppressing tubulin subunit off-rates[34].
473 Moreover, this role for Aurora kinase A in stabilizing spindle microtubules through BOD1L1 is
474 consistent with many tumor cells overexpressing or having hyperactive Aurora kinase A[35–37] and
475 also being CIN as a consequence of hyperstable k-MT attachments. Our observations suggest
476 that depending on the context, Aurora kinase A may destabilize k-MT attachments through direct
477 kinetochore substrate phosphorylation or stabilize k-MT attachments through indirect regulation
478 of PP2A activity.

479 Importantly, we found that the gene encoding BOD1L1 is occasionally altered in human
480 cancers. Most of these alterations are point mutations, but some amplifications and deletions also
481 occur (Figure 8A). In uterine endometrial cancer, the cancer that most commonly has BOD1L1
482 alterations, the alterations are associated with a reduced likelihood of death. The functional
483 consequence of these mutations remains unknown, although it is likely that at least some of them
484 cause a loss of BOD1L1 function. Thus, a reduced likelihood of death would be consistent with

485 our findings that BOD1L1 knockdown results in a loss of fitness of various tumor lines and
486 vulnerability to taxol or Aurora kinase A inhibitor (Figure 8C, 8D), which is corroborated by the
487 mitotic arrest and occasional mitotic catastrophe observed in cells with BOD1L1 knockdown
488 even in the absence of these drugs (Figure 5E, S3A). Since BOD1L1 also plays an important role
489 in the cellular response to DNA replication stress and DNA repair[16,19], these alterations may also
490 contribute to the loss of cell fitness through that role. In contrast to patients with uterine
491 endometrial cancer, alterations in BOD1L1 were associated with an increased risk of death in
492 lung adenocarcinoma and in skin cutaneous skin melanoma. The clinically differing impacts of
493 BOD1L1 alteration might depend on whether it is the mitotic functions and/or DNA repair
494 functions that have been altered relative to the alterations at the root of a specific type of cancer.
495 For example, both lung adenocarcinoma (if caused by smoking) and skin melanoma are driven
496 by DNA damage caused by chemicals or UV light, thus possibly highlighting the role of
497 BOD1L1 in DNA repair. Whereas in endometrial cancer, the cyclic high proliferation rate of this
498 tissue in fertile women might highlight the role of BOD1L1 in maintaining accurate mitosis and
499 avoiding CIN.
500 In summary, this work defines a new regulatory pathway in cells including Aurora kinase
501 A, BOD1L1 and PP2A that is required for timely mitotic progression, faithful chromosome
502 segregation, and regulation of proper microtubule stability. Our data expand on the previously
503 known role for BOD1L1 as well as the previously known role of Aurora kinase A and provide
504 insight into cellular responses that lead to adaptation to a small molecule suppressor of the CIN
505 phenotype.
506

507 **Methods**

508 Cell Culture

509 SW620, HCT116, HeLa and U20S cells were obtained from the ATCC. HEC1 cells were a gift
510 from Tyler Curiel. All cells were grown at 37°C in a humidified environment with 5% CO_2.
511 SW620, HeLa and U2OS cell lines were grown in Dulbecco's modified Eagle medium
512 (Corning® #15-017-CM) containing 10% FCS (Hyclone #82013-586), 250µg/L Amphotericin B
513 (VWR #82026-728), 50 U/mL penicillin and 50 µg/mL streptomycin (ThermoFisher Scientific
514 #15140122). HCT116 and HEC1 cells were grown in McCoy's 5A medium with the same
515 supplements. Cells were verified to be free of mycoplasma by frequent staining of plated cells
516 with DAPI. No contamination was observed.

517 Inhibitors and reagents

518 The CENP-E inhibitor GSK-923295 (MedChemExpress LLC # HY-10299) was used at 200 nM.
519 NOC (VWR #80058-500) was used at 100-500 ng/ml. STLC (Tocris #2191) was used at 25 µM.
520 ProTAME (Concept Life Sciences custom synthesis) was used at 25 µM. Okadaic acid (LC Labs
521 O-5857) was used at 200 nM. RO-3306 (Selleck #S7747) was used at 10 µM. AZ3146 (R&D
522 Systems #3994/10) was used at 2µM. BI2536 (Synthesized in-house) was used at 100
523 nM. MLN8237 (Selleck #S1133) was used at 10-50 nM. ZM447439 (Tocris Bioscience
524 #2458/10) was used at 2 µM. UMK57 (Aobious #AOB8668) was used at 100 nM.

525 Plasmids and cloning

526 The pLKO.1 – TRC cloning vector was a gift from David Root (Addgene plasmid # 10878;
527 http://n2t.net/addgene:10878 ; RRID:Addgene_10878). The shRNA sequences were cloned into
528 the AgeI and EcoRI sites of the plasmid using standard cloning techniques. The DNA constructs
529 were then verified by Sanger sequencing and amplified by maxiprep (Qiagen #12162).

530 Proteomic Screens

531 For the total protein and phospho-proteomic screen, ~80% confluent cells were re-plated at a
532 1:10 dilution on 15 cm plates. 3 dishes were treated with DMSO and 3 with UMK57. 72 hours
533 later, 2 dishes each of control and UMK57 treated cells were treated with 2.5 mM thymidine, and
534 continuing DMSO/UMK57 treatment. 24 hours following thymidine addition, it was washed out
535 with 2 washes of 5 ml PBS, and then fresh media added containing 100 ng/ml nocodazole, still
536 containing DMSO/UMK57. 16 hours later the DMSO treated cells were treated for 1 hour with
537 UMK57. The mitotic cells were harvested by shakeoff, centrifugation followed by a wash with 5
538 ml PBS, re-centrifugation and finally frozen at -80°C before mass spectrometry analysis.
539 Separately, following the 72 hours DMSO/UMK57 treatment, the remaining dishes were
540 trypsinized and re-plated on glass coverslips for microscopy analysis.

541 Sample preparation: Samples were prepared essentially as previously described[38,39], with a few
542 modifications. Cells were lysed in 8M urea, 200 mM EPPS, pH 8.5, supplemented with 1X
543 Pierce protease and phosphatase inhibitors. The resuspended samples were passed through a 1.5-
544 inch 21-gauge needle to ensure DNA were sheared. Protein concentration was determined for
545 each sample with BCA. Samples were reduced with 5 mM TCEP at room temperature for 20
546 min, alkylated with 10 mM iodoacetamide at room temperature for 20 min in the dark, and then
547 quenched with 10 mM DTT at room temperature for 20 min in the dark. Methanol-chloroform
548 precipitation was performed prior to protease digestion. In brief, 4-parts neat methanol were
549 added to each sample and vortexed, 1-part chloroform was added to the sample and vortexed,
550 and 3-parts water was added to the sample and vortexed. The sample was centrifuged at 14,000
551 RPM for 2 min at room temperature and subsequently washed once with 100% methanol.
552 Samples were resuspended in 200 mM EPPS, pH 8.5 and digested at room temperature for 14 h

553 with Lys-C protease at a 50:1 protein-to-protease ratio. Trypsin was then added at a 100:1
554 protein-to-protease ratio and the reaction was incubated for 6 h at 37°C.
555 Fe^{3}+-NTA phosphopeptide enrichment: Following digestion with Lys-C and trypsin, peptides
556 were desalted by using 100mg SepPak columns. The elutions were dried via vacuum
557 centrifugation and the phosphopeptides were enriched with the High-Select Fe3+-NTA
558 Phosphopeptide Enrichment Kit according to manufacturer's specifications using approximately
559 4 mg protein digest per enrichment column. The elutions were dried via vacuum centrifugation,
560 while the flow-throughs were saved for subsequent whole proteome analysis.
561 TMT labeling: In general, we estimate that at most 20 ug of phosphopeptides were enriched from
562 4 mg of total peptide. We added 40 ug of TMT 6-plex reagent (Thermo-Fisher) to the peptides
563 along with acetonitrile to again achieve a final acetonitrile concentration of approximately 30%
564 (v/v) in a total volume of 50 µL. Following incubation at room temperature for 1 h, the reaction
565 was quenched with hydroxylamine to a final concentration of 0.3% (v/v). The sample was
566 vacuum centrifuged to near dryness and subjected to C18 solid-phase extraction (SPE, Sep-Pak).
567 Off-line basic pH reversed-phase (BPRP) fractionation: We fractionated the peptide samples
568 using BPRP HPLC. We used an Agilent 1200 pump equipped with a degasser and a UV detector.
569 Peptides were subjected to a 50-min linear gradient from 5% to 35% acetonitrile in 10 mM
570 ammonium bicarbonate pH 8 at a flow rate of 0.6 mL/min over an Agilent 300Extend C18
571 column (3.5 µm particles, 4.6 mm ID and 250 mm in length). The peptide mixture was
572 fractionated into a total of 96 fractions, which were consolidated into 12 super-fractions.
573 Samples were subsequently acidified with 1% formic acid and vacuum centrifuged to near
574 dryness. Each consolidated fraction was desalted by StageTip, and reconstituted in 5%
575 acetonitrile, 5% formic acid for LC-MS/MS processing.

576 Liquid chromatography and tandem mass spectrometry: Mass spectrometric data were collected
577 on an Orbitrap Lumos mass spectrometer coupled to a Proxeon NanoLC-1200 UHPLC
578 (ThermoFisher Scientific). The 100 µm capillary column was packed in-house with 35 cm of
579 Accucore 150 resin (2.6 µm, 150Å; ThermoFisher Scientific). Data were acquired for 180 min
580 per fraction. MS1 spectra were acquired at 120 K resolving power for a maximum of 50 ms in
581 the Orbitrap, and features were filtered for monoisotopic peak assignment and charge states 2-6.
582 MS2 spectra were acquired by selecting the top 10 most abundant features. MS2 spectra were
583 acquired via collisional induced dissociation (CID), in the ion trap with an automatic gain control
584 (AGC) of 20K, quadrupole isolation width of 0.5 m/z and a maximum ion time of 120 ms with
585 Multistage Activation turned on. For MS3 acquisition, a synchronous precursor selection (SPS)
586 of 10 fragments ions was acquired for a maximum of 150 ms with an AGC of 300K and a
587 normalized collision energy of 65.
588 Data analysis: Database searching included all entries from the mouse UniProt Database
589 (downloaded: 2014). The database was concatenated with one composed of all protein sequences
590 for that database in the reversed order[40]. Raw files were converted to mzXML, and monoisotopic
591 peaks were re-assigned using Monocle[41]. Searches were performed with SEQUEST[42] using a 20-
592 ppm precursor ion tolerance. TMT labels on lysine residues and peptide N-termini (+229.1629
593 Da), as well as carbamidomethylation of cysteine residues (+57.021 Da) were set as static
594 modifications, while oxidation of methionine residues (+15.995 Da) and phosphorylation
595 (+79.966) were set as variable modifications. Peptide-spectrum matches (PSMs) were adjusted to
596 a 1% false discovery rate (FDR) using a linear discriminant after which proteins were assembled
597 further to a final protein-level FDR of 1% analysis[43]. Ascore was used to determine site
598 localization[44], with a score of 13 denoting 95% confidence for a specified phosphorylation site.

599 Phosphorylation sites were quantified by summing reporter ion counts across all matching PSMs.
600 Peptides were filtered to include only those with a summed signal-to-noise (SN) ≥ 100 across all
601 TMT channels as well as an isolation specificity ("isolation purity") of at least 0.5.

602 Whole Proteome Profiling

603 Sample preparation for whole proteome profiling: Flow-throughs from the phospho-enrichment
604 described above, 50 µg per replicate, were used for the whole proteome work for each sample.
605 TMT labeling: 120 µg of TMTpro reagents (Thermo-Fisher; Lot # WL338745) were added to
606 the peptides (50 µg) along with acetonitrile to achieve a final acetonitrile concentration of
607 approximately 30% (v/v) in a total volume of 100 µL. Following incubation at room temperature
608 for 1 h, the reaction was quenched with hydroxylamine to a final concentration of 0.3% (v/v).
609 The sample was vacuum centrifuged to near dryness and subjected to C18 solid-phase extraction
610 (SPE, Sep-Pak).
611 Off-line basic pH reversed-phase (BPRP) fractionation: We fractionated the peptide samples
612 using BPRP HPLC. We used an Agilent 1200 pump equipped with a degasser and a UV detector.
613 Peptides were subjected to a 50-min linear gradient from 5% to 35% acetonitrile in 10 mM
614 ammonium bicarbonate pH 8 at a flow rate of 0.6 mL/min over an Agilent 300Extend C18
615 column (3.5 µm particles, 4.6 mm ID and 250 mm in length). The peptide mixture was
616 fractionated into a total of 96 fractions, which were consolidated into 24 super-fractions (in a
617 checkerboard-like pattern) of which 12 were used for data acquisition. Samples were
618 subsequently acidified with 1% formic acid and vacuum centrifuged to near dryness. Each
619 consolidated fraction was desalted by StageTip, and reconstituted in 5% acetonitrile, 5% formic
620 acid for LC-MS/MS processing.

621 Liquid chromatography and tandem mass spectrometry. Mass spectrometric data were collected
622 on an Orbitrap Fusion mass spectrometer coupled to a Proxeon NanoLC-1200 UHPLC
623 (ThermoFisher Scientific). A 100 µm capillary column was packed in-house with 35 cm of
624 Accucore 150 resin (2.6 µm, 150Å; ThermoFisher Scientific). Data were acquired for 180 min
625 per fraction. MS1 spectra were acquired at 120 K resolving power for a maximum of 100 ms in
626 the Orbitrap, and features were filtered for monoisotopic peak assignment and charge state of 2.
627 MS2 spectra were acquired by selecting the top 10 most abundant features. MS2 spectra were
628 acquired via collisional induced dissociation (CID), in the ion trap with an automatic gain control
629 (AGC) of 9K, quadrupole isolation width of 0.7 m/z at Rapid Scan Rate. For MS3 acquisition, a
630 synchronous precursor selection (SPS) of 10 fragments ions was acquired for a maximum of 200
631 ms with an AGC of 200K and a normalized collision energy of 55.
632 Data analysis. Searches were performed as described above but without phosphorylation variable
633 modifications. Proteins were quantified by summing reporter ion counts across all matching
634 PSMs. More specifically, reporter ion intensities were adjusted to correct for the isotopic
635 impurities of the different TMTpro reagents according to manufacturer specifications. Peptides
636 were filtered to include only those with a summed signal-to-noise (SN) ≥ 100 across all TMT
637 channels and isolation specificity of at least 0.5. The signal-to-noise (S/N) measurements of
638 peptides assigned to each protein were summed (for a given protein) and each protein abundance
639 measurement was scaled, such that the summed signal-to-noise for that protein across all
640 channels equals 100, thereby generating a relative abundance (RA) measurement.
641 Transfections
642 200,000 SW620 cells were plated on glass coverslips in 12-well plates. 24 hours following
643 plating, they were transfected with 1 µg plasmid DNA and 2.5 µl Lipofectamine™ 2000

644 (ThermoFisher #11668027) in a total of 1 ml Opti-MEM™ media (ThermoFisher #31985070).
645 Four hours following transfection, the media was changed for DMEM containing 2μg/ml
646 puromycin. The cells were then assayed 48-72 hours following addition of puromycin.

647 SDS-PAGE and Western blot

648 Gels and blots were performed as described previously [45]. Prior to loading samples on gel, 4X
649 Laemmli buffer (200 mM Tris pH 6.8, 4% SDS, 40% glycerol, 4% 2-mercaptoethanol, 0.12
650 mg/ml bromophenol blue) was added to a final dilution of 1X, and the samples were boiled for 5
651 minutes. Proteins were separated on SDS-PAGE gel using stacking gel (4% 29:1 acrylamide:
652 Bis-acrylamide, 125mM Tris pH 6.8, 0.1% SDS, 0.1% ammonium persulfate, 0.1% TEMED)
653 and (8-15% 29:1 acrylamide: Bis-acrylamide, 400 mM Tris pH 8.8, 0.1% SDS, 0.1% ammonium
654 persulfate, 0.1% TEMED) at 120V until the bromophenol blue has run off or longer, as needed.
655 Transfer onto nitrocellulose membrane was performed for at least 24 hours at 30V under wet
656 conditions in 1X transfer buffer (14.4 g/L glycine, 3.0 g/L Tris, 20% methanol). Conditions for
657 western blots includes the use of 5% nonfat dry milk in TBS-T 0.5% (50 mM Tris [pH 7.2], 150
658 mM NaCl, 0.5% Tween 20) for blocking and TBS-T 0.5% for washing. 4 washes for 10 minutes
659 each were performed after primary and secondary antibody incubation periods. The bands were
660 visualized by enhanced chemiluminescence using Clarity (Bio-Rad #1705060) using a Bio-Rad
661 ChemiDoc MP.

662 Immunoprecipitation

663 Protein-G beads were first crosslinked to the antibody by incubating the beads and antibody
664 overnight on a rotating platform. The beads were then washed with PBS and then crosslinking
665 solution (20mM dimethyl pimelimidate, 0.3M HEPES in ice cold water). The beads were then
666 incubated in crosslink solution for 10 minutes at room temperature. The solution is then

667 discarded, and the incubation repeated in fresh crosslink buffer, which is performed three times.
668 The beads are then washed in PBS twice and twice with lysis buffer prior to use.
669 SW620 cells from confluent 15 cm dishes were split 1:5. 48 hours later, 2.5 mM thymidine was
670 added. 24 hours following thymidine addition, it was washed out with 2 5ml washes with PBS.
671 Fresh media containing 100 ng/ml nocodazole was then added. 16 hours later, the cells were
672 harvested by scraping, washed once with cold PBS, and lysed in the following buffer: 0.5%
673 NP40, 100 mM NaCl, 50 mM tris pH 7.4, 10 mM glycerol 2-phosphate. Cells were lysed on ice
674 for 20 minutes before centrifuging at 15,000 x g for 20 minutes at 4ºC. The supernatant was
675 transferred to a fresh tube, and input sample set aside. 10 µl of packed volume protein G beads
676 cross-linked to antibody were added to each sample for 2 hours on a rotating platform at 4ºC.
677 The beads were then washed 5 times in lysis buffer and dried using a 30 g needle attached to a
678 vacuum line. 30-100 µl of 1X sample buffer were added to the beads before elution by boiling
679 and loading on gel.
680 Identification of BOD1L1 interacting proteins
681 Excised gel bands were cut into approximately 1 mm^3 pieces. Gel pieces were then subjected to a
682 modified in-gel trypsin digestion procedure[46]. Gel pieces were washed and dehydrated with
683 acetonitrile for 10 min. followed by removal of acetonitrile. Pieces were then completely dried in
684 a speed-vac. Rehydration of the gel pieces was with 50 mM ammonium bicarbonate solution
685 containing 12.5 ng/µl modified sequencing-grade trypsin (Promega, Madison, WI) at 4ºC. After
686 45 min., the excess trypsin solution was removed and replaced with 50 mM ammonium
687 bicarbonate solution to just cover the gel pieces. Samples were then placed in a 37ºC room
688 overnight. Peptides were later extracted by removing the ammonium bicarbonate solution,
689 followed by one wash with a solution containing 50% acetonitrile and 1% formic acid. The

690 extracts were then dried in a speed-vac (~1 hr). The samples were then stored at 4ºC until
691 analysis. On the day of analysis the samples were reconstituted in 5 – 10 µl of HPLC solvent A
692 (2.5% acetonitrile, 0.1% formic acid). A nano-scale reverse-phase HPLC capillary column was
693 created by packing 2.6 µm C18 spherical silica beads into a fused silica capillary (100 µm inner
694 diameter x ~30 cm length) with a flame-drawn tip[47]. After equilibrating the column each sample
695 was loaded via a Famos auto sampler (LC Packings, San Francisco CA) onto the column. A
696 gradient was formed and peptides were eluted with increasing concentrations of solvent B
697 (97.5% acetonitrile, 0.1% formic acid). As peptides eluted they were subjected to electrospray
698 ionization and then entered into an LTQ Orbitrap Velos Pro ion-trap mass spectrometer (Thermo
699 Fisher Scientific, Waltham, MA). Peptides were detected, isolated, and fragmented to produce a
700 tandem mass spectrum of specific fragment ions for each peptide. Peptide sequences (and hence
701 protein identity) were determined by matching protein databases with the acquired fragmentation
702 pattern by the software program, Sequest (Thermo Fisher Scientific, Waltham, MA)[42]. All
703 databases include a reversed version of all the sequences and the data was filtered to between a
704 one and two percent peptide false discovery rate.

705 GST pulldowns

706 We performed GST-pulldowns essentially as described previously[19]. Briefly, SW620 mitotic
707 nuclear extracts were incubated with 1 µg of GST-fusion protein or purified GST as a control on
708 a rotating platform for 3 hours. Bound proteins were then purified via binding to glutathione
709 Sepharose (GE Healthcare) and washed. Samples were then analyzed by Western blot.

710 RNA interference

711 Gene knockdown was performed by cloning the following shRNA sequences into the PLKO1
712 vector and then transfecting cells with 1µg of plasmid DNA and 2.5µl lipofectamine 2000 per ml

713 according to the manufacturer's directions. Media was changed after 5 hours, and puromycin
714 added after 24 hours.
715 BOD1L1-1: 5'- GCCAATGATGCCATGTCGATA-3'
716 BOD1L1-2: 5'- ACTCGCATGTATCCAAGTAAA-3'
717 Immunofluorescence
718 Following treatments, cells were pre-extracted in PHEM buffer (60 mM PIPES, 25 mM HEPES,
719 pH 6.9, 10 mM EGTA, and 4 mM $MgSO_4$, 1% Triton X-100, 10 mM glycerol 2-phosphate) for
720 10 minutes at 4°C and then fixed in 4% paraformaldehyde in PBs at room temperature for 20
721 minutes. The remaining steps were performed at room temperature. The cells were then washed
722 twice with PBS for before blocking with ADB (10% serum, 0.1% Triton X-100 in PBS) for 15
723 minutes. Primary antibodies were then diluted in ADB and used at the indicated dilution.
724 Secondary antibodies were diluted in ADB. After incubation with antibodies, the cells were
725 washed three times with PBS 0.1% Triton X-100. Finally, the cells were counterstained with
726 DAPI and mounted on slides using ProLong™ Gold antifade reagent (ThermoFisher Scientific
727 #P36934).
728 Microscopy
729 Images were acquired with a Nikon Eclipse Ti microscope equipped with a cooled charge-
730 coupled device Clara camera (Andor Technology) controlled by Nikon NIS-Elements software
731 version 4.30.02. Images were acquired in 0.15-0.4 μm sections using a plan apo 1.4 numerical
732 aperture 100X (kinetochore analysis) or 60X (lagging chromosome analysis) oil-immersion
733 objective using 1X1 binning. Samples were illuminated using an X-cite light source (Excelitas
734 Technologies Corp). All image analysis, adjustment and cropping was performed using Fiji
735 software [48]. Image deconvolution was performed using Nikon Elements batch deconvolution

736 software version 5.21.00 on automatic mode. All kinetochore intensity analysis was performed
737 on the raw images, except for microtubule intensity determination for which deconvolution was
738 performed prior to analysis. Line scans were performed on the deconvoluted images in Fiji and
739 the data was then exported to Graphpad Prism. All images of BOD1L1 selected for presentation
740 are deconvolved single optical slices. Images of other stained proteins are deconvolved
741 maximum intensity projections. Where shown, insets are from single optical Z-slices. Images
742 were selected to represent the mean quantified data. Quantification of kinetochore staining
743 intensity was performed by first determining the brightest plane for which a given kinetochore
744 appears. Then, an outline was drawn using the ellipse tool. The integrated intensity was
745 determined by multiplying the average intensity by the area of the kinetochore. Background
746 levels of staining were determined by saturating the brightness and contrast settings to find the
747 darkest spot within the chromatin containing area and were subtracted from the intensity of the
748 kinetochore. Aurora kinase A pT288 was quantified by first creating a sum projection of the
749 image. Then, an outline was drawn around the whole cell, and the fluorescence intensity
750 measured. The background-subtracted, normalized integrated intensities for all cells were then
751 plotted. To quantify levels of cold-stable microtubules, images were first deconvolved. Then, A
752 sum-intensity projection was created in Fiji. Viewing the ACA channel, a rectangle was drawn
753 that was 2 μm wide in the pole-pole axis, and as long as the furthest centromeres in the
754 metaphase plate. Then, switching to the tubulin channel, the average tubulin intensity was
755 measured in the rectangle. From the average intensity value, the minimum intensity value was
756 used as the background level and subtracted. The Background-subtracted intensity values were
757 then averaged across all of the cells that were analyzed for each condition and experimental
758 repeat.

759 For live-cell microscopy, cells were transfected with 0.5 μg of mCherry-H2B-expressing plasmid
760 together with pLKO vectors. After selection with puromycin, the cells were washed twice with
761 PBS, given fresh medium and moved to a Tokai Hit incubation chamber with CO_2 and
762 temperature control on the microscope. The cells were imaged every 5 minutes at 20X
763 magnification for 48 hours with 2X2 binning.

764 Antibodies

765 The following antibodies were used for immunofluorescence (IF) and/or immunoblotting (IB):
766 human anti-ACA (Geisel School of Medicine; IF at 1:2000), mouse anti-Hec1 (Santa Cruz C-11;
767 IF,IB at 1:1000), mouse anti-PP2AR1A (Santa Cruz SC-74580; IB at 1:500), mouse anti-
768 PP2AC (Santa Cruz SC-166034; IB at 1:500), rabbit anti-PP2A B56 Alpha
769 (MyBioSource.com MBS8524809; IB at 1:500), mouse anti-PP2A B56 Beta (Santa Cruz E-6; IB
770 at 1:500), mouse anti-PP2A B56 Gamma (Santa Cruz A-11; IB at 1:500), mouse anti-PP2A B56
771 Delta (Santa Cruz H-11; IB at 1:500), rabbit anti-PP2A B56 Epsilon (Aviva Systems Biology
772 RP56694_P050; IB at 1:500), rabbit anti-Hec1 pS44 (gift of Jennifer DeLuca; IF at 1:500)[49],
773 rabbit anti DSN1 pS100 (gift of Iain Cheeseman; IF at 1:250)[50], rabbit anti-KNL1 pT943/pT1155
774 (Cell Signaling #40758), mouse anti-α-Tubulin DM1α (Sigma-Aldrich; IF at 1:4000-1:10,000),
775 mouse anti-Aurora A (Cell Signaling Technology 1F8; IF at1:1000), Rabbit anti-Aurora A
776 pT288 (Cell Signaling Technology C39D8; IF at 1:500), Rabbit anti-TACC3 (gift of Jordan
777 Raff; IF at 1:1000)[51], mouse anti-TPX2 (Cell Signaling Technology D9Y1V; IF at 1:1000),
778 rabbit anti-Aurora B pT232 (Rockland 600-401-677; IF/IB at 1:1000), rabbit anti-MCAK pS95
779 (Abcam #AB74146; IF/IB at 1:500), rabbit anti-Hec1 pT31[26] (IF at 1:100,000, WB at 1:1000),
780 rabbit anti-BOD1L1 (IF at 1:1000) (gift of Grant Stewart[16]), rabbit anti-BOD1L1 (Genetex
781 #GTX119946; WB at 1:500). Secondary antibodies used were highly cross-adsorbed Alexa

782 Fluor® 488, 594 and 647 raised in donkey or goat (Invitrogen; IF at 1:1000), horseradish
783 peroxidase (Bio-Rad; IB at 1:10000-10,0000), Mouse TrueBlot® ULTRA: rat Anti-Mouse IgG
784 (Rockland 18-8817-33; IB at 1:1000), Anti-IgG (H+L) Goat Polyclonal Antibody (Horseradish
785 Peroxidase), Peroxidase AffiniPure Goat Anti-Rabbit IgG (H+L) (IB at 1:5000), Goat Polyclonal
786 Antibody (Horseradish Peroxidase), Peroxidase AffiniPure Goat Anti-Mouse IgG (H+L) (IB at
787 1:5000).

788 Statistical analysis of cell biology data

789 All statistical tests were performed using Graphpad Prism version 8.4.2. Except where indicated,
790 all experiments were performed as 2-3 independent biological repeats. In most IF experiments,
791 20 cells per repeat were analyzed, and 25 kinetochores for each cell measured. Experiments with
792 other numbers are noted in the figure legends. For anaphase error rates, 100 anaphases per
793 condition were assessed for each of 3 independent biological experiments. Statistical significance
794 was calculated between indicated conditions using two-tailed *t*-tests or Dunnett's multiple
795 comparison test. For these tests, the data distribution was assumed to be normal but this was not
796 formally tested.

797 Study population data, and statistical analysis

798 The cBioPortal for Cancer Genomics was used to query and visualize *BOD1L1* alterations in
799 data from The Cancer Genome Atlas (TCGA). Then, TCGA PanCancer Atlas cancer specific
800 clinical and *BOD1L1* alteration data was downloaded via cBioPortal for Cancer Genomics for
801 cancer types where *BOD1L1* alteration was most frequent: uterine corpus endometrial carcinoma
802 TCGA-UCEC PCA (n= 529), lung adenocarcinoma TCGA-LUAD (n = 667), cutaneous
803 melanoma TCGA-SKCM (n = 448), stomach adenocarcinoma TCGA-STAD (n = 440), and lung
804 squamous cell carcinoma TCGA-LUSC (n = 487). All statistical analysis was conducted in R

805 version 4.2.1. Survival analysis using Kaplan-Meier plots and Cox Proportional-Hazards models
806 was conducted using R package *survival* and plotted using R package *survminer*. Univariate
807 Kaplan-Meier survival strata were plotted for altered *BOD1L1* status in each cancer type to
808 assess five-year overall survival status. Cox Proportional Hazards models for each cancer type
809 tested association of *BOD1L1* alteration status with adjustment for patient age, sex (excepting
810 uterine), and tumor stage or grade. Using Fisher's exact tests and patient data from all TCGA-
811 PanCancer Atlas cancer datasets (n = 10,967 from 32 cancer types), we tested whether *BOD1L1*
812 alterations were exclusive of alterations to other Aurora A-BOD1L1- PP2A gene pathway
813 members.

814 Data availability

815 The cell biology datasets generated during and/or analysed during the current study are available
816 from the corresponding author on reasonable request. The MS datasets will be uploaded to an
817 appropriate public repository upon acceptance of the article.

818

Acknowledgements

We thank Grant Stewart, Jennifer Delucca, Iain Cheeseman, Tyler Curiel, Jose Teodoro and Adrian Saurin for providing reagents. We also thank Sanjukta Guha Thakurta (Thermo Fisher Center for multiplexed proteomics, Harvard University) and Ross Tomaino (Taplin Mass Spectrometry Facility, Harvard University) for assistance with the proteomics analysis. We also thank the members of the Compton laboratory for helpful discussions and feedback. TJK was supported by fellowships from the Fonds de Recherche du Québec – Santé and the Canadian Institutes of Health Research. This work was also supported by grants from the National Institutes of Health #GM051542 to DAC. The authors acknowledge the following Shared Resources facilities (Bio-Rad ChemiDoc MP) at the Norris Cotton Cancer Center at Dartmouth with NCI Cancer Center Support Grant 5P30 CA023108-40.

Author Contributions

Conceptualization: DAC and TJK. Investigation: TJK, IMV, MRH. Formal analysis: TJK, IMV. Methodology: TJK, DAC. Funding acquisition: TJK, DAC. Supervision: BCC, DAC. Writing- original draft: TJK. Writing- review & editing: TJK, MRH, BCC, DAC. Project administration: DAC.

Competing interests

The authors declare that they have no conflicts of interest

Materials & Correspondence

Any requests should be addressed to DAC

840 **References**

841 1. Luo, J., Solimini, N. L. & Elledge, S. J. Principles of Cancer Therapy: Oncogene and Non-
842 oncogene Addiction. *Cell* **136**, 823–837 (2009).
843 2. Geigl, J. B., Obenauf, A. C., Schwarzbraun, T. & Speicher, M. R. Defining 'chromosomal
844 instability'. *Trends Genet.* **24**, 64–69 (2008).
845 3. Lengauer, C., Kinzler, K. W. & Vogelstein, B. Genetic instability in colorectal cancers.
846 *Nature* **386**, 623–627 (1997).
847 4. Thompson, S. L. & Compton, D. A. Chromosome missegregation in human cells arises
848 through specific types of kinetochore-microtubule attachment errors. *Proc. Natl. Acad. Sci.*
849 **108**, 17974–17978 (2011).
850 5. Bakhoum, S. F., Thompson, S. L., Manning, A. L. & Compton, D. A. Genome stability is
851 ensured by temporal control of kinetochore–microtubule dynamics. *Nat. Cell Biol.* **11**, 27–35
852 (2009).
853 6. Kleyman, M., Kabeche, L. & Compton, D. A. STAG2 promotes error correction in mitosis by
854 regulating kinetochore-microtubule attachments. *J. Cell Sci.* jcs.151613 (2014)
855 doi:10.1242/jcs.151613.
856 7. Bakhoum, S. F., Genovese, G. & Compton, D. A. Deviant Kinetochore Microtubule
857 Dynamics Underlie Chromosomal Instability. *Curr. Biol.* **19**, 1937–1942 (2009).
858 8. Bakhoum, S. F., Kabeche, L., Murnane, J. P., Zaki, B. I. & Compton, D. A. DNA-Damage
859 Response during Mitosis Induces Whole-Chromosome Missegregation. *Cancer Discov.* **4**,
860 1281–1289 (2014).
861 9. Hunter, A. W. *et al.* The Kinesin-Related Protein MCAK Is a Microtubule Depolymerase that
862 Forms an ATP-Hydrolyzing Complex at Microtubule Ends. *Mol. Cell* **11**, 445–457 (2003).

863 10. Maney, T., Hunter, A. W., Wagenbach, M. & Wordeman, L. Mitotic Centromere–
864 associated Kinesin Is Important for Anaphase Chromosome Segregation. *J. Cell Biol.* **142**,
865 787–801 (1998).
866 11. Orr, B., Talje, L., Liu, Z., Kwok, B. H. & Compton, D. A. Adaptive Resistance to an
867 Inhibitor of Chromosomal Instability in Human Cancer Cells. *Cell Rep.* **17**, 1755–1763
868 (2016).
869 12. Huang, H. *et al.* Tripin/hSgo2 recruits MCAK to the inner centromere to correct defective
870 kinetochore attachments. *J. Cell Biol.* **177**, 413–424 (2007).
871 13. Tanno, Y. *et al.* Phosphorylation of mammalian Sgo2 by Aurora B recruits PP2A and
872 MCAK to centromeres. *Genes Dev.* **24**, 2169–2179 (2010).
873 14. Kettenbach, A. N. *et al.* Quantitative Phosphoproteomics Identifies Substrates and
874 Functional Modules of Aurora and Polo-Like Kinase Activities in Mitotic Cells. *Sci. Signal.* **4**,
875 rs5–rs5 (2011).
876 15. Arslanhan, M. D., Rauniyar, N., Yates, J. R. & Firat-Karalar, E. N. Aurora Kinase A
877 proximity map reveals centriolar satellites as regulators of its ciliary function. *EMBO Rep.* **22**,
878 (2021).
879 16. Higgs, M. R. *et al.* BOD1L Is Required to Suppress Deleterious Resection of Stressed
880 Replication Forks. *Mol. Cell* **59**, 462–477 (2015).
881 17. Moustafa-Kamal, M., Gamache, I., Lu, Y., Li, S. & Teodoro, J. G. BimEL is
882 phosphorylated at mitosis by Aurora A and targeted for degradation by βTrCP1. *Cell Death*
883 *Differ.* **20**, 1393–1403 (2013).
884 18. Kufer, T. A. *et al.* Human TPX2 is required for targeting Aurora-A kinase to the spindle.
885 *J. Cell Biol.* **158**, 617–623 (2002).

886 19. Bayley, R. *et al.* H3K4 methylation by SETD1A/BOD1L facilitates RIF1-dependent
887 NHEJ. *Mol. Cell* **82**, 1924-1939.e10 (2022).
888 20. Higgs, M. R. *et al.* Histone Methylation by SETD1A Protects Nascent DNA through the
889 Nucleosome Chaperone Activity of FANCD2. *Mol. Cell* **71**, 25-41.e6 (2018).
890 21. Porter, I. M. *et al.* Bod1, a novel kinetochore protein required for chromosome
891 biorientation. *J. Cell Biol.* **179**, 187–197 (2007).
892 22. Porter, I. M., Schleicher, K., Porter, M. & Swedlow, J. R. Bod1 regulates protein
893 phosphatase 2A at mitotic kinetochores. *Nat. Commun.* **4**, 2677 (2013).
894 23. Schleicher, K., Porter, M., Sundaramoorthy, R., Porter, I. M. & Swedlow, J. R. The
895 Ndc80 complex targets Bod1 to human mitotic kinetochores. 14.
896 24. Kazyken, D. *et al.* AMPK directly activates mTORC2 to promote cell survival during
897 acute energetic stress. *Sci. Signal.* **12**, eaav3249 (2019).
898 25. McKinley, K. L. & Cheeseman, I. M. Large-Scale Analysis of CRISPR/Cas9 Cell-Cycle
899 Knockouts Reveals the Diversity of p53-Dependent Responses to Cell-Cycle Defects. *Dev.*
900 *Cell* **40**, 405-420.e2 (2017).
901 26. Kucharski, T. J. Chromosome segregation fidelity is controlled by small changes in
902 phospho-occupancy at the kinetochore-microtubule interface. *J. Cell Biol.* (2022).
903 27. Sobajima, T. *et al.* PP6 regulation of Aurora A–TPX2 limits NDC80 phosphorylation and
904 mitotic spindle size. *J. Cell Biol.* **222**, e202205117 (2023).
905 28. Zaytsev, A. V. *et al.* Multisite phosphorylation of the NDC80 complex gradually tunes its
906 microtubule-binding affinity. *Mol. Biol. Cell* **26**, 1829–1844 (2015).
907 29. Herman, J. A. *et al.* Hyper-active RAS/MAPK introduces cancer-specific mitotic
908 vulnerabilities. *Proc. Natl. Acad. Sci.* **119**, e2208255119 (2022).

909 30. DeLuca, K. F. *et al.* Aurora A kinase phosphorylates Hec1 to regulate metaphase
910 kinetochore–microtubule dynamics. *J. Cell Biol.* **217**, 163–177 (2018).
911 31. Ye, A. A. *et al.* Aurora A Kinase Contributes to a Pole-Based Error Correction Pathway.
912 *Curr. Biol.* **25**, 1842–1851 (2015).
913 32. Campbell, C. S. & Desai, A. Tension sensing by Aurora B kinase is independent of
914 survivin-based centromere localization. *Nature* **497**, 118–121 (2013).
915 33. Zhang, R., Roostalu, J., Surrey, T. & Nogales, E. Structural insight into TPX2-stimulated
916 microtubule assembly. *eLife* **6**, e30959 (2017).
917 34. Reid, T. A. *et al.* Suppression of microtubule assembly kinetics by the mitotic protein
918 TPX2. *J. Cell Sci.* jcs.178806 (2016) doi:10.1242/jcs.178806.
919 35. Bischoff, J. R. A homologue of Drosophila aurora kinase is oncogenic and amplified in
920 human colorectal cancers. *EMBO J.* **17**, 3052–3065 (1998).
921 36. Zhou, H. *et al.* Tumour amplified kinase STK15/BTAK induces centrosome
922 amplification, aneuploidy and transformation. *Nat. Genet.* **20**, 189–193 (1998).
923 37. Sen, S., Zhou, H. & White, R. A. A putative serine/threonine kinase encoding gene
924 BTAK on chromosome 20q13 is ampli®ed and overexpressed in human breast cancer cell
925 lines.
926 38. Navarrete-Perea, J., Yu, Q., Gygi, S. P. & Paulo, J. A. Streamlined Tandem Mass Tag
927 (SL-TMT) Protocol: An Efficient Strategy for Quantitative (Phospho)proteome Profiling
928 Using Tandem Mass Tag-Synchronous Precursor Selection-MS3. *J Proteome Res* (2018).
929 39. Li, J. *et al.* TMTpro-18plex: The Expanded and Complete Set of TMTpro Reagents for
930 Sample Multiplexing. *J Proteome Res* (2021).

931 40. Elias, J. E. & Gygi, S. P. Target-decoy search strategy for increased confidence in large-
932 scale protein identifications by mass spectrometry. *Nat. Methods* **4**, 207–214 (2007).
933 41. Rad, R. *et al.* Improved Monoisotopic Mass Estimation for Deeper Proteome Coverage. *J*
934 *Proteome Res* (2021).
935 42. Yates, J. R. An approach to correlate tandem mass spectral data of peptides with amino
936 acid sequences in a protein database.
937 43. Huttlin, E. L. A Tissue-Specific Atlas of Mouse Protein Phosphorylation and Expression.
938 44. Beausoleil, S. A., Villen, J., Gerber, S. A., Rush, J. & Gygi, S. P. A probability-based
939 approach for high-throughput protein phosphorylation analysis and site localization. *Nat.*
940 *Biotechnol.* **24**, (2006).
941 45. Kucharski, T. J., Minshall, P. E., Moustafa-Kamal, M., Turnell, A. S. & Teodoro, J. G.
942 Reciprocal Regulation between 53BP1 and the Anaphase-Promoting Complex/Cyclosome Is
943 Required for Genomic Stability during Mitotic Stress. *Cell Rep.* **18**, 1982–1995 (2017).
944 46. Shevchenko, A., Wilm, M., Vorm, O. & Mann, M. Mass Spectrometric Sequencing of
945 Proteins from Silver-Stained Polyacrylamide Gels. *Anal. Chem.* **68**, 850–858 (1996).
946 47. Peng, J. & Gygi, S. P. Proteomics: the move to mixtures. *J. Mass Spectrom.* **36**, 1083–
947 1091 (2001).
948 48. Schindelin, J. *et al.* Fiji: an open-source platform for biological-image analysis. *Nat.*
949 *Methods* **9**, 676–682 (2012).
950 49. DeLuca, K. F., Lens, S. M. A. & DeLuca, J. G. Temporal changes in Hec1
951 phosphorylation control kinetochore-microtubule attachment stability during mitosis. *J. Cell*
952 *Sci.* **124**, 622–634 (2011).

953 50. Welburn, J. P. I. *et al.* Aurora B Phosphorylates Spatially Distinct Targets to
954 Differentially Regulate the Kinetochore-Microtubule Interface. *Mol. Cell* **38**, 383–392 (2010).
955 51. Gergely, F. *et al.* The TACC domain identifies a family of centrosomal proteins that can
956 interact with microtubules. *Proc. Natl. Acad. Sci.* **97**, 14352–14357 (2000).
957
958

959 **Figure legends**

960 **Figure 1: Proteomic screening reveals BOD1L1 as a mediator of UMK57 adaptation**

961 A) Cartoon illustration depicting the experimental scheme used to discover mediators of
962 UMK57 adaptation. SW620 cells were first treated for 3 days with UMK57 or DMSO
963 control. They were then synchronized by thymidine-nocodazole treatment. The DMSO
964 control sample was then treated with UMK57 for the final hour before harvest. The cells
965 were then collected and analyzed by mass spectrometry.

966 B) SW620 cells were prepared as in (A) but re-plated on glass coverslips instead of
967 synchronization. After 24 hours, the cells were fixed and stained for Hec1 and DAPI. The
968 rate of lagging chromosomes was then assessed. Statistical significance was calculated using
969 Dunnett's multiple comparison test. Representative images from 3 independent experiments
970 are shown. The images were adjusted evenly for brightness and contrast for presentation. The
971 scale bar is 10μm.

972 C) SW620 cells were prepared as in (A) and analyzed by mass spectrometry. The number of
973 peptides and proteins detected in the screens are shown.

974 D) Proteins from the phospho-proteomic screen that were significantly changed ($p < 0.1$) by
975 Student's *t*-test were analyzed for gene ontology. The data were then transferred to Prism
976 software and plotted.

977 E) Proteins from the phospho-proteomic screen that were significantly changed ($p < 0.1$) by
978 Student's *t*-test were analyzed by PhosphositePlus for sequence motif enrichment and
979 plotted.

980 F) Volcano plot analysis of the phospho-proteomic screen results. Proteins of potential interest
981 are highlighted in orange. Statistical significance was calculated using two-tailed *t*-tests.

982 G) Analysis of overlap between the phospho-proteomic study presented here and a previous
983 study[14]. Proteins with changes in phosphorylation greater than 4-fold caused by Aurora A or
984 Aurora B kinase inhibitors were considered targets of Aurora A or Aurora B kinase. The list
985 of Aurora A and Aurora B targets was compared to the list of proteins from the phospho-
986 proteomic screen that had a significantly changed phosphorylation site ($p < 0.1$) by Student's
987 *t*-test.
988 H) Cartoon drawing of the FAM44 protein family, showing the Bod1 similar domain and
989 potential Aurora A kinase sites on BOD1L1. Scales are approximate.
990 I) Amino acid sequence alignment of BOD1L1 orthologs from residues 2933-2992 (relative to
991 the human sequence). Residues highlighted in pink indicate Aurora kinase defining motifs.
992 Residues highlighted in yellow indicate potential phosphorylation sites.
993 **Figure 2: BOD1L1 and Aurora A are required for adaptation to UMK57**
994 A) SW620 cells were transfected with control shRNA or shRNA against BOD1L1 and selected
995 with puromycin. Following selection, the cells were fixed and stained for Hec1 and DAPI.
996 Control cells were treated with DMSO and cells adapted to UMK57 were treated for 72
997 hours. Cells treated acutely with UMK57 were treated for 1 hour. The percentage of lagging
998 chromosomes in anaphase for cells expressing the indicated shRNA is shown. 100 cells per
999 shRNA and condition were scored for the presence of lagging chromosomes for each of 3
1000 independent biological repeats. Error bars indicate the mean +/- SEM. * denotes $p < 0.05$,
1001 *** denotes $p < 0.001$. Statistical significance was calculated between the indicated
1002 conditions using Dunnett's multiple comparison test.
1003 B) SW620 cells were transfected with control shRNA or shRNA against BOD1L1 and selected
1004 with puromycin. Following selection, the cells were fixed and stained for Hec1 and DAPI.

1005 Control cells were treated with DMSO, and cells adapted to UMK57 were treated for 72
1006 hours. Cells treated acutely with UMK57 were treated for 1 hour. The cells were then fixed
1007 and stained for Hec1 and DAPI. Representative images from 3 independent experiments are
1008 shown. The images were adjusted evenly for brightness and contrast for presentation. The
1009 scale bars of main images are 10 μm, and insets are 1 μm.

1010 C) SW620 cells were plated. 24 hours following plating, DMSO or 50 nM MLN8237 was
1011 added, with or without 100 nM UMK57. After 72 hours, the cells were fixed and stained for
1012 Hec1 and DAPI. The percentage of lagging chromosomes in anaphase for cells expressing
1013 the indicated shRNA is shown. 100 cells per shRNA and condition were scored for the
1014 presence of lagging chromosomes for each of 3 independent biological repeats. Error bars
1015 indicate the mean +/- SEM. * denotes $p < 0.05$, *** denotes $p < 0.001$. Statistical
1016 significance was calculated between the indicated conditions using Dunnett's multiple
1017 comparison test.

1018 D) SW620 cells were transfected with control shRNA or shRNA against BOD1L1 and selected
1019 with puromycin. Following selection, the cells were treated with DMSO or Okadaic acid as
1020 indicated for 90 minutes prior to fixation. The cells were then stained for Hec1 and DAPI.
1021 The percentage of lagging chromosomes in anaphase for cells expressing the indicated
1022 shRNA is shown. 100 cells per shRNA and condition were scored for the presence of lagging
1023 chromosomes for each of 3 independent biological repeats. Error bars indicate the mean +/-
1024 SEM. * denotes $p < 0.05$, *** denotes $p < 0.001$. Statistical significance was calculated
1025 between the indicated conditions using Dunnett's multiple comparison test.

1026 **Figure 3: Microtubule destabilization mediated by hyperactive MCAK enhances Aurora**
1027 **A/TPX2 localization to the mitotic spindle**

1028 A) Immunofluorescence images from an asynchronous population of SW620 cells treated either
1029 with DMSO control, acute (1 hour) UMK57 or UMK57 for 3 days. The cells were then fixed
1030 and stained for total Aurora A and Aurora A pT288. The Aurora A and Aurora A pT288
1031 were adjusted evenly for brightness and contrast for presentation. The DAPI channel of each
1032 condition was adjusted independently. Representative images from 2 independent biological
1033 experiments are shown. The scale bars are 10 μm.
1034 B) Quantification of the relative spindle protein intensities from the conditions from panel (A).
1035 The levels of the prometaphase DMSO conditions was set to 1 and the other conditions
1036 shown as fold-changes. The fluorescence levels for at least 30 cells for each of 2 independent
1037 biological repeats were measured. Error bars indicate the mean +/- SEM. Statistical
1038 significance was calculated between the indicated conditions using Dunnett's multiple
1039 comparison test.
1040 C) Cells were prepared as for panel (A) but stained for TPX2 and alpha tubulin.
1041 D) Cells were prepared as for panel (A) but stained for TACC3 and tubulin.
1042 E) Quantification of the relative spindle protein intensities from panels (C) and (D). The tubulin
1043 intensities from panels (C) and (D) were combined into a single plot.
1044 **Figure 4: BOD1L1 localizes to the mitotic spindle and kinetochores during mitosis**
1045 A) Immunofluorescence images from an asynchronous population of SW620 cells in various
1046 stages of mitosis stained for BOD1L1, Hec1 and DAPI. The BOD1L1 and Hec1 channels
1047 were adjusted evenly for brightness and contrast for presentation. The DAPI channel of each
1048 condition was adjusted independently. Representative images from 2 independent biological
1049 experiments are shown. The scale bars of main images are 10 μm, and insets are 1 μm.

1050 B) Immunofluorescence images from an asynchronous population of SW620 cells in various
1051 stages of mitosis stained for BOD1L1, alpha tubulin and DAPI. The BOD1L1 and alpha
1052 tubulin channels were adjusted evenly for brightness and contrast for presentation. The DAPI
1053 channel of each condition was adjusted independently. Representative images from 2
1054 independent biological experiments are shown. The scale bars of main images are 10 μm,
1055 and insets are 1 μm.
1056 C) Immunofluorescence images from an asynchronous population of SW620 cells in various
1057 stages of mitosis stained for BOD1L1, Aurora A and DAPI. The BOD1L1 and Hec1
1058 channels were adjusted evenly for brightness and contrast for presentation. The DAPI
1059 channel of each condition was adjusted independently. Representative images from 2
1060 independent biological experiments are shown. The scale bars of main images are 10 μm,
1061 and insets are 1 μm.
1062 **Figure 5: BOD1L1 is required for correct k-MT attachment stability and faithful**
1063 **chromosome segregation**
1064 A) Immunofluorescence images of SW620 cells were transfected with control shRNA or shRNA
1065 against BOD1L1 and selected with puromycin. The cells were then fixed and stained for
1066 alpha tubulin and ACA. Representative images of 2 independent biological experiments are
1067 shown. The images were adjusted evenly for brightness and contrast for presentation. The
1068 scale bar is 10μm.
1069 B) Quantification of the cells shown in panel (A). Statistical significance was calculated
1070 between the indicated conditions using Dunnett's multiple comparison test.
1071 C) SW620 cells were co-transfected with control shRNA or shRNA against BOD1L1 together
1072 with mCherry-H2B and selected with puromycin. Following selection, time lapse imaging

1073 was started at 5-minute intervals. The fate of at least 40 cells per experiment for each of 3
1074 independent biological repeats was recorded. Statistical significance was calculated between
1075 the indicated conditions using Dunnett's multiple comparison test.

1076 D) Immunofluorescence images of SW620 cells were transfected with control shRNA or shRNA
1077 against BOD1L1 and selected with puromycin. The cells were then placed at 4ºC for 15
1078 minutes before they were fixed and stained for alpha tubulin and ACA. Representative
1079 images of 3 independent biological experiments are shown. The images were adjusted evenly
1080 for brightness and contrast for presentation. The scale bar is 10μm.

1081 E) Quantification of the relative intensity of alpha Tubulin from the conditions shown in panel
1082 (D). The levels of prometaphase shC expressing cells were set to 1 and the other conditions
1083 shown as a fold-change. At least 50 cells per condition from each of 3 independent biological
1084 experiments were quantified. Error bars indicate the mean +/- SEM. **** denotes $p <$
1085 0.0001. Statistical significance was calculated between the indicated conditions using
1086 Dunnett's multiple comparison test.

1087 **Figure 6: BOD1L1 interacts with the PP2A-B56 phosphatase complex**

1088 A) Cartoon illustration depicting the experimental scheme used to discover protein interactors of
1089 BOD1L1. SW620 cells were first synchronized by thymidine-nocodazole. BOD1L1 was then
1090 immunoprecipitated and purified along with interacting proteins. The samples were then
1091 separated by SDS-PAGE. The entire lanes were excised and cut into 5 pieces and analyzed
1092 by mass spectrometry. The experiment was performed once.

1093 B) Table of selected interacting proteins detected in the control immunoprecipitation and
1094 BOD1L1 immunoprecipitations showing the number of detected peptides.

1095 C) SW620 cells were prepared as in panel (A), except that they were analyzed by Western blot.
1096 BOD1L1 was immunoprecipitated and the purified proteins were then separated by SDS-
1097 PAGE, transferred to nitrocellulose membrane and blotted as indicated. The panels were
1098 adjusted for brightness and contrast for presentation. An experiment representative of two
1099 independent biological repeats is shown.
1100 D) SW620 mitotic nuclear cell extracts were incubated with GST or GST-BOD1L fragments.
1101 Complexes were then isolated by glutathione-sepharose and analyzed by Western blot. The
1102 blot shown is representative of 2 independent experiments.
1103 **Figure 7: BOD1L1 expression is required for normal kinetochore phosphorylation**
1104 A) Immunofluorescence images from an asynchronous population of SW620 cells transfected
1105 with control shRNA or shRNA against BOD1L1 in prometaphase or metaphase and stained
1106 for Hec1, Hec1 pT31 and DAPI. The BOD1L1 and Hec1 channels were adjusted evenly for
1107 brightness and contrast for presentation. The DAPI channel of each condition was adjusted
1108 independently. Representative images from 2 independent biological experiments are shown.
1109 The scale bars of main images are 10 μm, and insets are 1 μm.
1110 B) As for panel (A), except for KNL1 pMELT/ACA instead of Hec1 pT31/total Hec1
1111 C) Quantification of the relative kinetochore pT31 Hec1/Hec1 intensities from the conditions
1112 from panel (A). The condition with the lowest level of pT31 Hec1/Hec1 was set to 1 and the
1113 other conditions shown as fold-changes. 25 kinetochores were quantified from each of 20
1114 cells for each of 2 independent biological repeats. Error bars indicate the mean +/- SEM.
1115 Statistical significance was calculated between the indicated conditions using Dunnett's
1116 multiple comparison test.
1117 D) As for panel (C), except for Hec1 pS44/total Hec1instead of Hec1 pT31/total Hec1

1118 E) As for panel (C), except for Hec1 pS55/total Hec1 instead of Hec1 pT31/total Hec1

1119 F) As for panel (C), except for DSN1 pS109/ACA instead of Hec1 pT31/total Hec1

1120 G) As for panel (C), except for KNL1 pMELT/ACA instead of Hec1 pT31/total Hec1

1121 H) As for panel (C), except for MCAK pS95/ACA instead of Hec1 pT31/total Hec1

1122 I) As for panel (C), except for Aurora B pT232/ACA instead of Hec1 pT31/total Hec1

1123 J) Quantification of total cellular Aurora A pT288/Total Aurora A. The condition with the
1124 lowest level of pT31 Hec1/Hec1 was set to 1 and the other conditions shown as fold-changes.
1125 The level of protein was measured from at least 25 cells for each of 2 independent biological
1126 repeats. Error bars indicate the mean +/- SEM. Statistical significance was calculated
1127 between the indicated conditions using Dunnett's multiple comparison test.

1128 **Figure 8: BOD1L1 is mutated in human cancers**

1129 A) The 10,967 sequenced cancers in the TCGA were queried for the presence of mutations in
1130 the *BOD1L1* gene and plotted by cancer subtype.

1131 B) Kaplan-Meier five-year overall survival by *BOD1L1* alteration status with Cox-Proportional
1132 Hazards Ratios and 95% confidence intervals from models adjusted for potential confounders
1133 (age, sex [except uterine], and tumor grade or stage). A) Uterine corpus endometrial
1134 carcinoma TCGA-UCEC, n= 529; b) lung adenocarcinoma TCGA-LUAD, n = 667; c)
1135 cutaneous melanoma TCGA-SKCM, n = 448; d) stomach adenocarcinoma TCGA-STAD, n
1136 = 440; e) lung squamous cell carcinoma TCGA-LUSC, n = 487.

1137 C) U2OS, HCT116, SW620 and HeLa cells were plated. They were then transfected with
1138 control shRNA or shRNA against BOD1L1 and selected with puromycin in the presence of
1139 compounds as indicated. After 1 week of selection, the cells were fixed and stained with

1140 crystal violet. Representative images from 3 independent experiments are shown. The scale
1141 bar is 4 cm.
1142 D) Quantification of cells from (C). The staining intensity of the cells was measured using Fiji
1143 and plotted. Error bars indicate the mean +/- SEM. Statistical significance was calculated
1144 between the indicated conditions using Student's *t*- test.
1145 E) Cartoon illustration showing a possible mechanism for adaptation to UMK57. UMK57
1146 agonizes MCAK, resulting in lower k-MT stability, which is sensed by Aurora A. Aurora A
1147 then phosphorylates BOD1L1, releasing PP2A to reduce phosphorylation of the NDC80
1148 complex, resulting in higher k-MT stability.
1149 **Figure S1: Changes in UMK57 adapted cells; Adaptation to UMK57 does not happen**
1150 **through changes to protein level**
1151 A) SW620 cells were first treated for 3 days with UMK57 or DMSO control. They were then re-
1152 plated on glass coverslips. After 24 hours, the cells were fixed and stained for Aurora B
1153 pT232, ACA and DAPI. A single experiment was performed. The scale bar is 10µm.
1154 B) SW620 cells were prepared as in (A) but stained for MCAK pS95 and ACA. A single
1155 experiment was performed. The scale bar is 10µm.
1156 C) Quantification of the relative kinetochore pT232 Aurora B/ACA intensities from the
1157 conditions from panel (A). The condition with the lowest level of pT232 Aurora B/ACA was
1158 set to 1 and the other conditions shown as fold-changes. 30 kinetochores were quantified
1159 from each of 20 cells from a single experiment. Error bars indicate the mean +/- SEM.
1160 Statistical significance was calculated between the indicated conditions using Dunnett's
1161 multiple comparison test.

1162 D) As for C but quantifying the relative kinetochore pS95 MCAK/ACA intensities from panel
1163 (B).
1164 E) Volcano plot analysis of the total protein level proteomic screen results. Proteins of potential
1165 interest are highlighted in orange. Statistical significance was calculated using two-tailed *t*-
1166 tests.
1167 F) STRING analysis of the statistically significant ($p < 0.1$) top-100 positively changed
1168 phosphorylated proteins and top-100 negatively changed phospho-proteins showing gene
1169 association networks.
1170 G) SW620 cells were first treated for 3 days with UMK57 or DMSO control. They were then
1171 allowed to remain asynchronous or were synchronized by thymidine-nocodazole. The cells
1172 were then harvested and lysed. The proteins were separated by SDS-PAGE, transferred to
1173 nitrocellulose membrane and finally blotted as indicated. The shown blots are representative
1174 of 3 independent experiments.
1175 **Figure S2: Validation of BOD1L1 antibody and shRNAs; BOD1L1 does not require**
1176 **Aurora A, Aurora B signaling or microtubules for kinetochore localization**
1177 A) SW620 cells were transfected with control shRNA or shRNA against BOD1L1 and selected
1178 with puromycin. The cells were then harvested at the indicated time points, lysed and the
1179 proteins separated by SDS-PAGE. They were then transferred to nitrocellulose membrane
1180 and blotted as indicated.
1181 B) Immunofluorescence images from an asynchronous population of SW620 transfected with
1182 control shRNA or shRNA against BOD1L1 and selected with puromycin. The cells were
1183 stained for BOD1L1, Hec1 and DAPI. The BOD1L1 and Hec1 channels were adjusted
1184 evenly for brightness and contrast for presentation. The DAPI channel of each condition was

1185 adjusted independently. Representative images from 2 independent biological experiments
1186 are shown. The scale bars of main images are 10 μm, and insets are 1 μm.
1187 C) SW620 cells were plated. 24 hours following plating, various concentrations of MLN8237
1188 were added as indicated. Following 3 days of treatment, the cells were fixed and stained with
1189 crystal violet. Representative images from 2 independent experiments are shown. The scale
1190 bar is 4 cm.
1191 D) Immunofluorescence images from an asynchronous population of SW620 transfected with
1192 control shRNA or shRNA against BOD1L1 and selected with puromycin. The cells were
1193 overnight with the indicated concentrations of nocodazole. The cells were then fized and
1194 stained for BOD1L1, Hec1 and DAPI. The BOD1L1 and Hec1 channels were adjusted
1195 evenly for brightness and contrast for presentation. The DAPI channel of each condition was
1196 adjusted independently. Representative images from 2 independent biological experiments
1197 are shown. The scale bars of main images are 10 μm, and insets are 1 μm.
1198 E) Immunofluorescence images from an asynchronous population of SW620 transfected with
1199 control shRNA or shRNA against BOD1L1 and selected with puromycin. The cells were
1200 then treated with DMSO control or Aurora A or Aurora B inhibitors for 90 minutes prior to
1201 fixation. The cells were stained for BOD1L1, Hec1 and DAPI. The BOD1L1 and Hec1
1202 channels were adjusted evenly for brightness and contrast for presentation. The DAPI
1203 channel of each condition was adjusted independently. Representative images from 2
1204 independent biological experiments are shown. The scale bars of main images are 10 μm,
1205 and insets are 1 μm.
1206 **Figure S3: Still images of live-cell movies; Hec1 is not required for BOD1L1 localization to**
1207 **kinetochores**

1208 A) SW620 cells were co-transfected with control shRNA or shRNA against BOD1L1 together
1209 with mCherry-H2B and selected with puromycin. After 72 hours of selection, time lapse
1210 imaging was started at 5-minute intervals. Representative Images from 3 independent
1211 experiments are shown. The images were independently adjusted for brightness and contrast
1212 for presentation. The scale bars are 10 μm.
1213 B) HeLa cells were plated on glass coverslips. 24 hours after plating, doxycycline or water was
1214 added to the wells. 48 hours following addition of doxycycline, the cells were fixed and
1215 stained as indicated. Representative Images from 2 independent experiments are shown. The
1216 images were independently adjusted for brightness and contrast for presentation. The scale
1217 bars of main images are 10 μm, and insets are 1 μm.
1218 **Figure S4: Mutations in BOD1L1 are mutually exclusive from mutations in other pathway**
1219 **components.**
1220 A) The 10,967 sequenced cancers in the TCGA were queried for the presence of mutations in
1221 the *BOD1L1*, *Aurora A, TPX2, PPP2CA, PPP2CB, PPP2R1A, PPP2R1B, PPP2R5A,*
1222 *PPP2R5B, PPP2R5C, PPP2R5D, PPP2R5E* genes and plotted by cancer subtype.
1223 B) The 10,967 sequenced cancers in the TCGA were queried for the presence of mutations in
1224 *BOD1L1*, *Aurora A, TPX2, PPP2CA, PPP2CB, PPP2R1A, PPP2R1B, PPP2R5A, PPP2R5B,*
1225 *PPP2R5C, PPP2R5D, PPP2R5E* and plotted showing the ovelap of alterations..
1226 C) Mutual exclusivity between genes in *BOD1L1* and the other queried genes was tested by
1227 *BOD1L1* alteration versus alteration to any other gene pathway member (Fisher's exact
1228 P=1.3E-24), and *BOD1L1* alteration versus each of the eleven gene pathway members
1229 independently.

1230 D) U2OS, HCT116, SW620 and HeLa cells were plated. They were then transfected with
1231 control shRNA or shRNA against BOD1L1. 24 hours post-transfection, puromycin was
1232 added. 72 hours after addition of puromycin, the cells were harvested by scraping and lysed.
1233 The proteins were then separated by SDS-PAGE and transferred to nitrocellulose membrane
1234 and finally blotted as indicated.
1235 E) U2OS, HCT116, HEC1 and HeLa cells were plated. They were then transfected with control
1236 shRNA or shRNA against BOD1L1 and selected with puromycin. After 3 days of selection,
1237 the cells were fixed and stained with Hec1 and DAPI and the rates of lagging chromosomes
1238 were assessed from100 anaphases for each 3 independent experiments. Error bars indicate
1239 the mean +/- SEM. Statistical significance was calculated between the indicated conditions
1240 using Student's *t*- test.
1241 F) U2OS or SW620 cells were plated. They were then transfected with control shRNA or
1242 shRNA against BOD1L1 and selected with puromycin. After 3 days of selection, the cells
1243 were fixed and stained with Hec1 and DAPI and the percentage of cells with micronuclei was
1244 determined. At least 1000 cells were examined per condition for each 3 independent
1245 experiments. Error bars indicate the mean +/- SEM. Statistical significance was calculated
1246 between the indicated conditions using Student's *t*- test.
1247 G) Cells were prepared as in figure 7C. Following fixation, the cells were imaged by brightfield
1248 microscopy. Representative images of 3 independent experiments are shown. The scale bar is
1249 100 μm.
1250

Kucharski et al. Figure 1

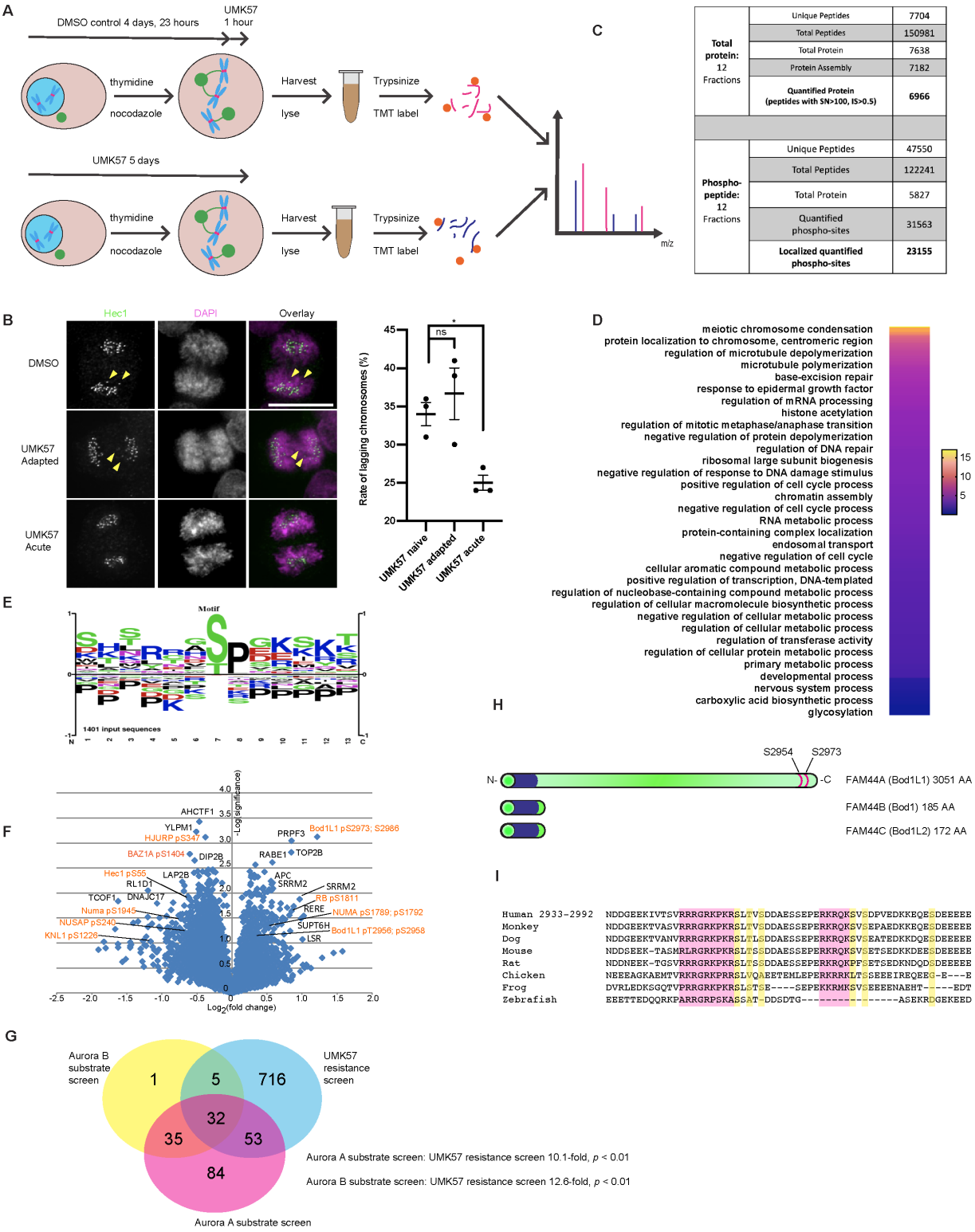

1251

Kucharski et al. Figure S1

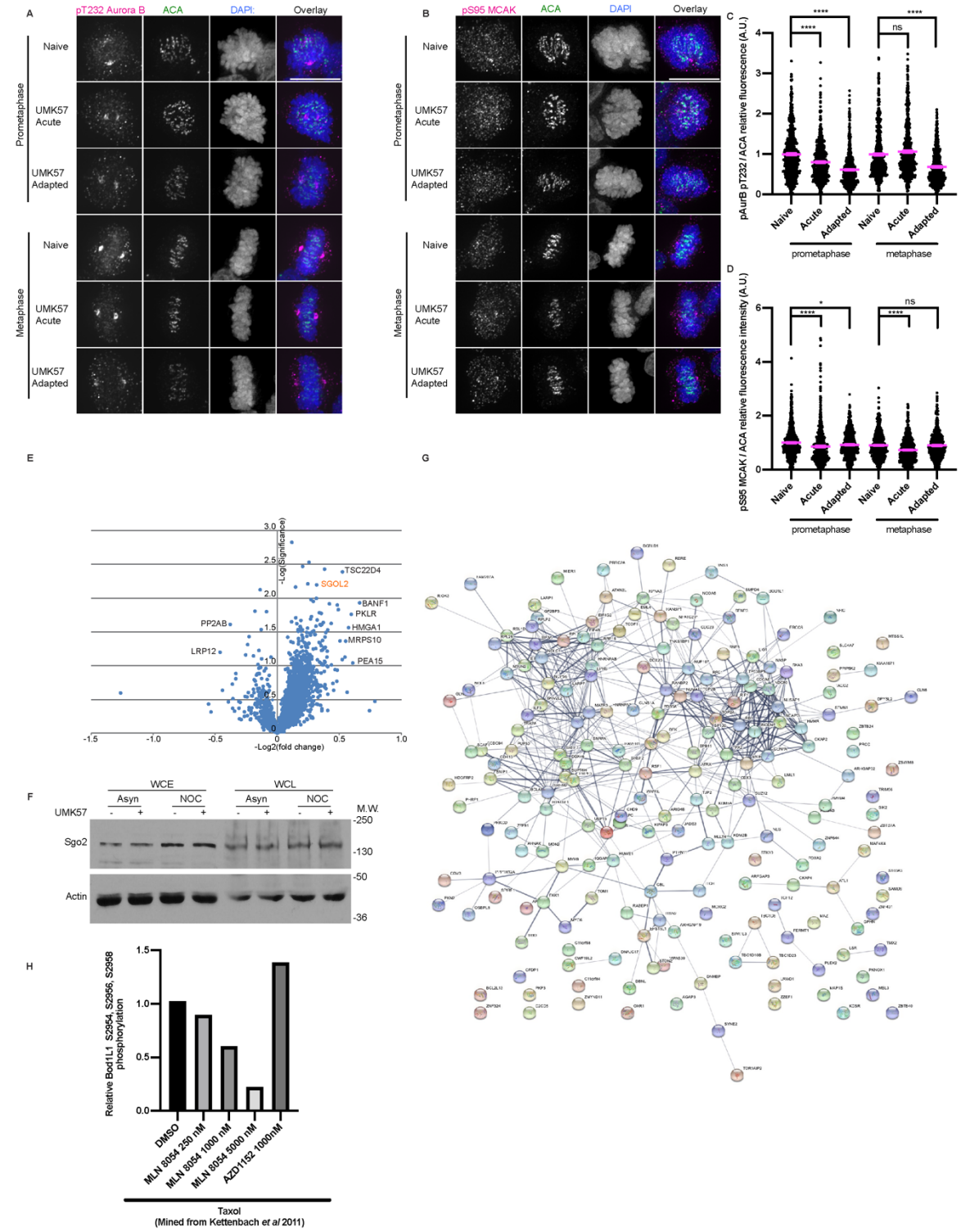

1255

1256

Kucharski et al. Figure 2

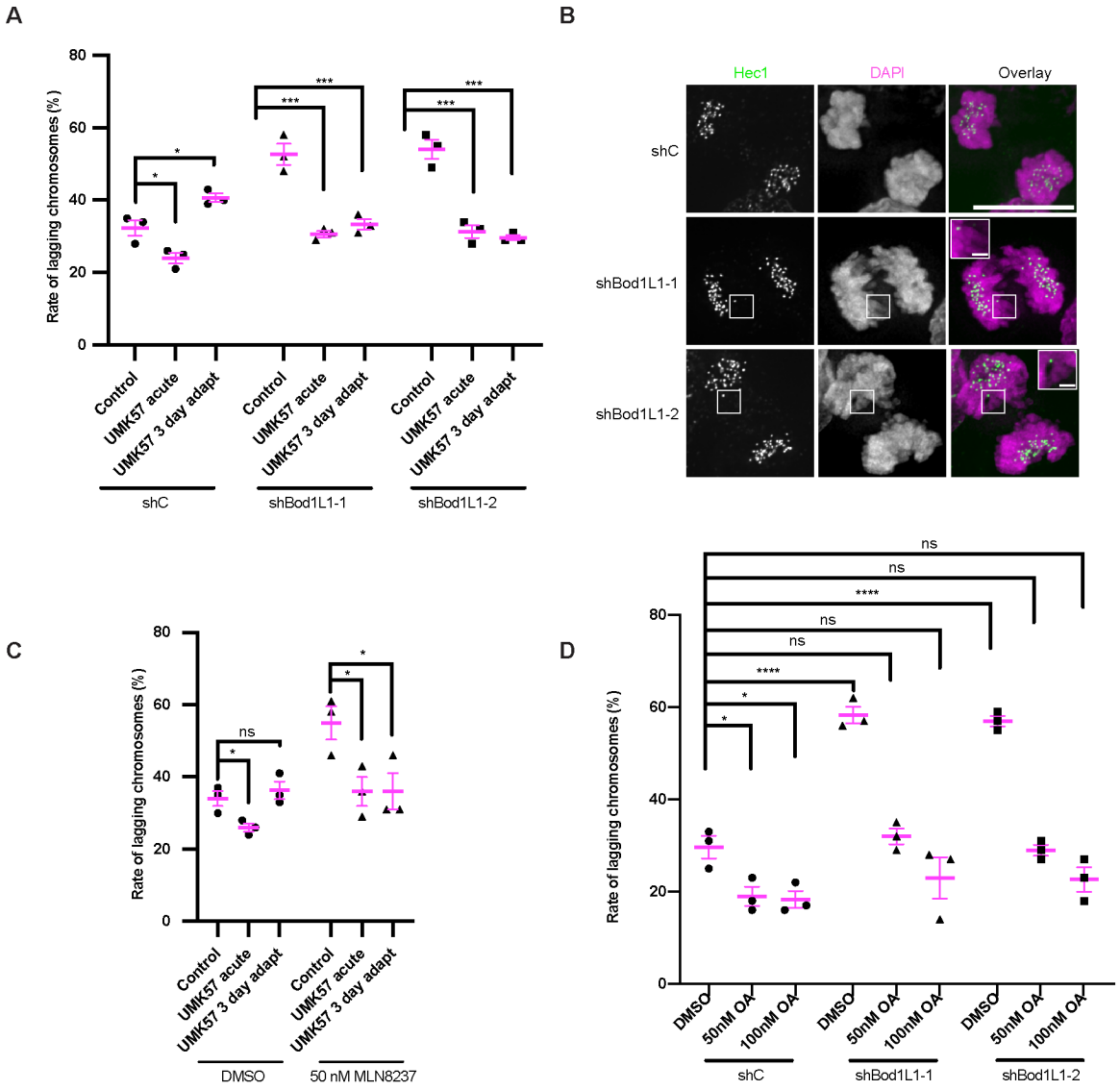

1257

1258

1259

Kucharski et al. Figure 3

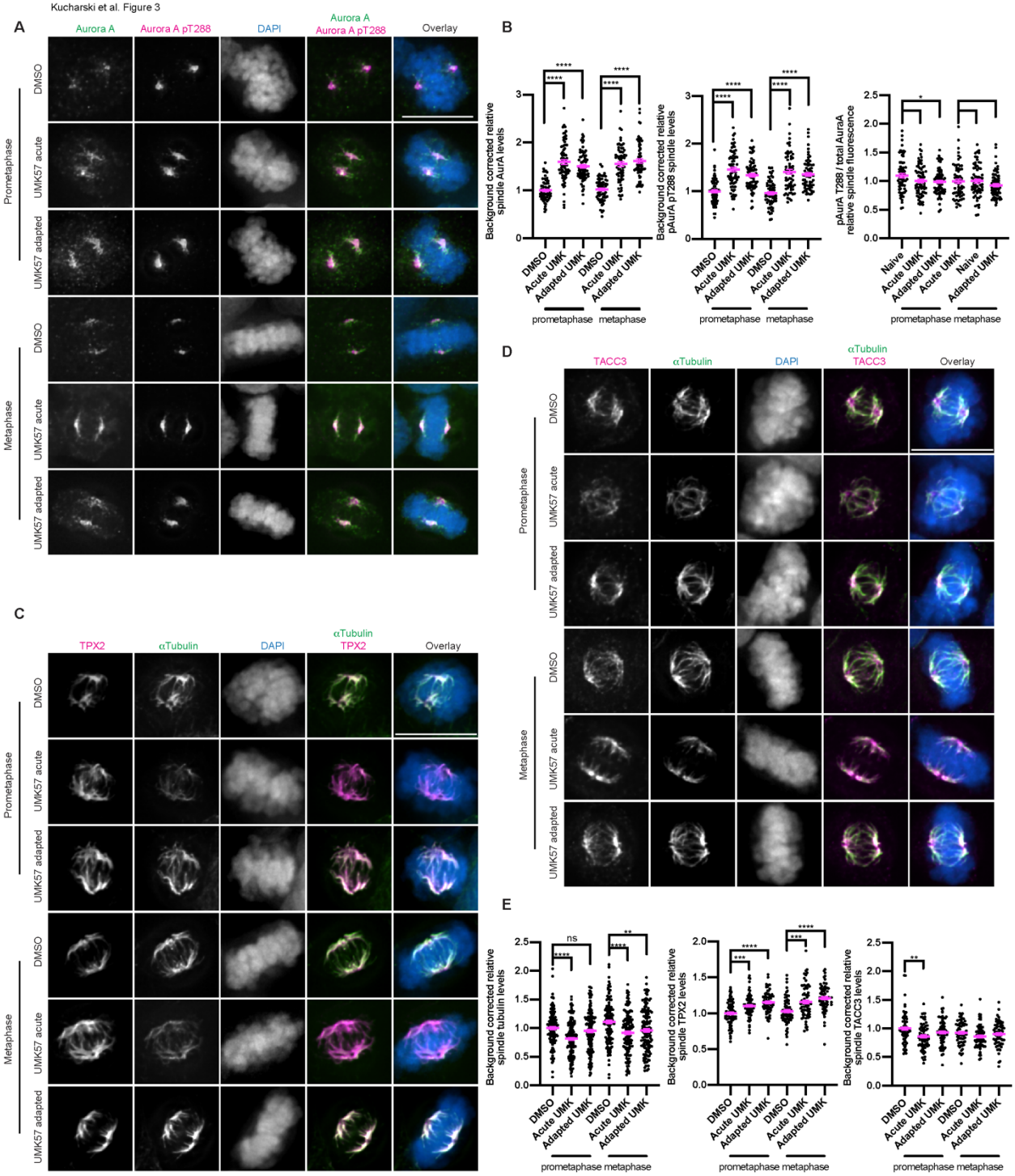

1260

Kucharski et al. Figure S2

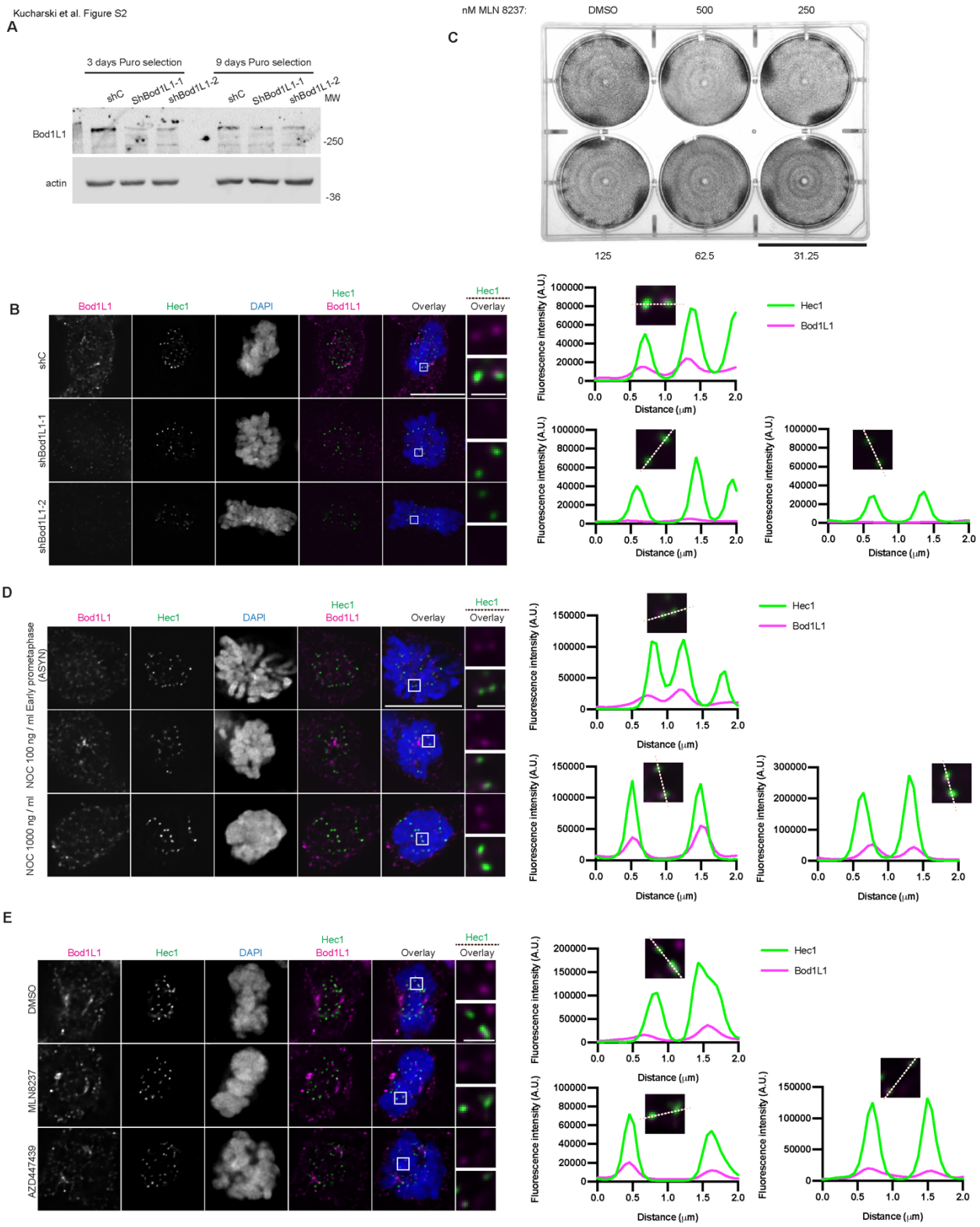

1261

1262

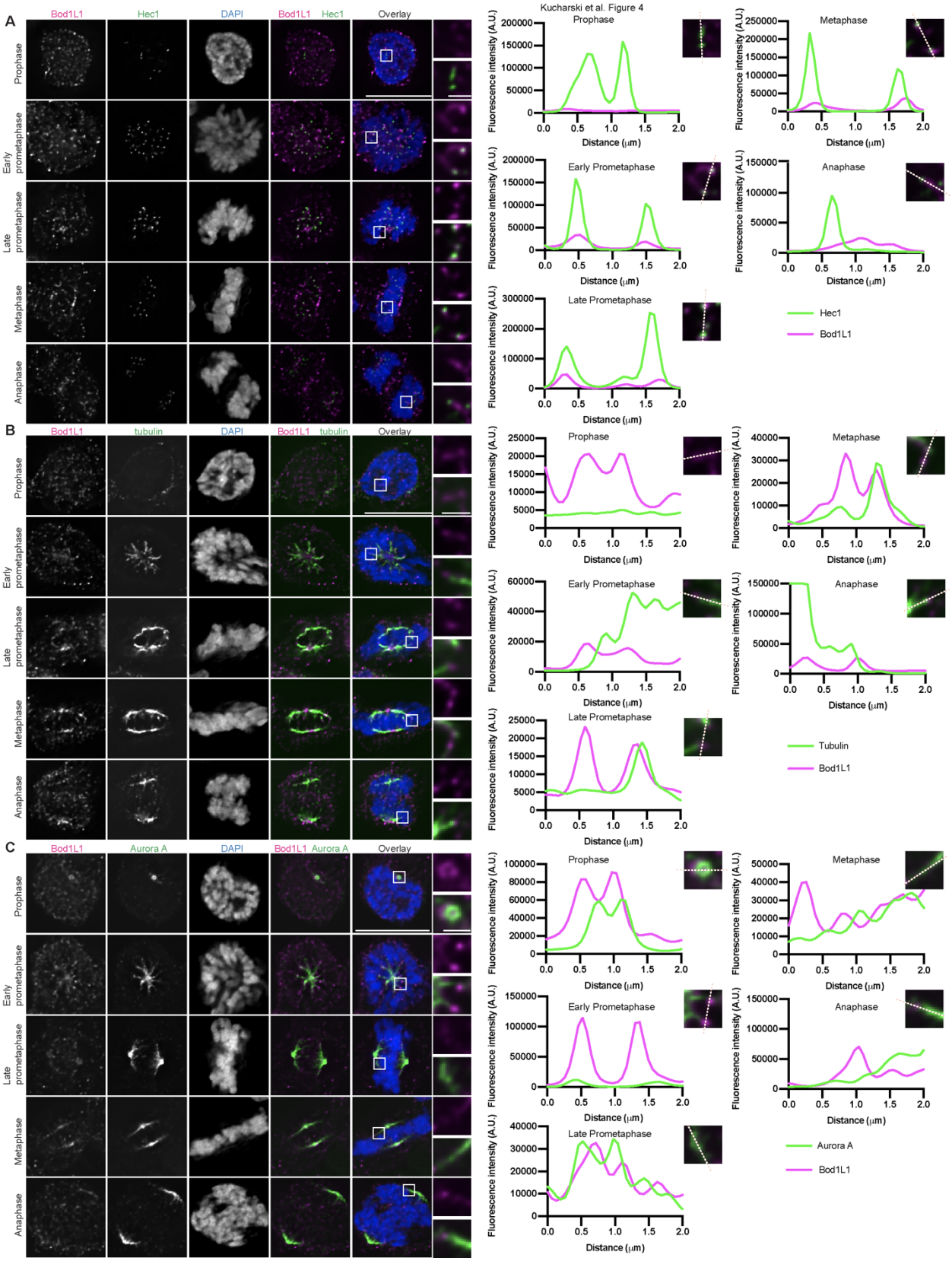
Kucharski et al. Figure 4
A
Bod1L1
Hec1
DAPI
Bod1L1 Hec1
Overlay
Prophase
Early prometaphase
Late prometaphase
Metaphase
Anaphase
Fluorescence intensity (A.U.)
Distance (μm)
Hec1
Bod1L1
B
tubulin
Bod1L1 tubulin
Tubulin
C
Aurora A
Bod1L1 Aurora A
Aurora A

1263

Kucharski et al. Figure 5

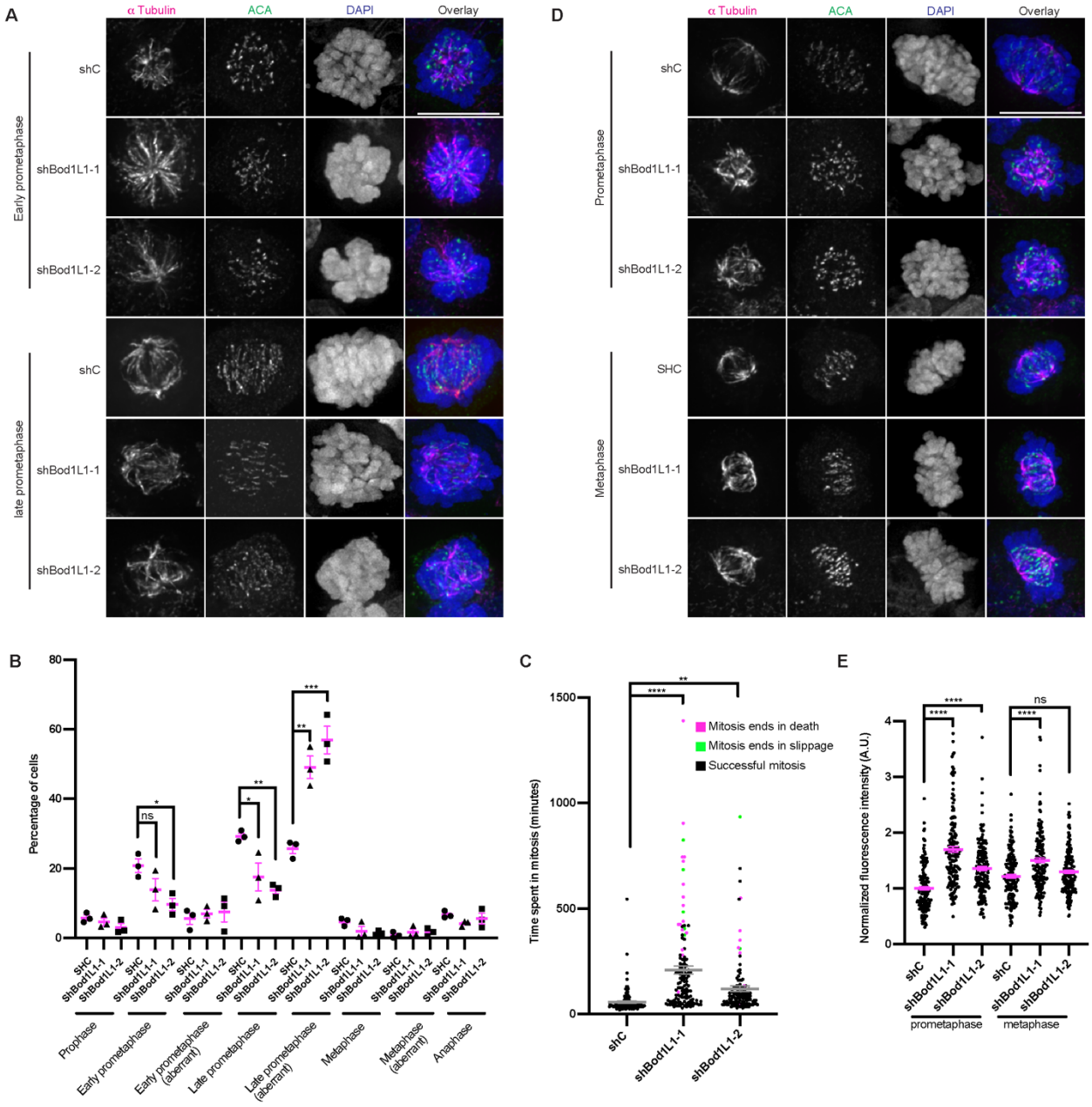

1264

Kucharski et al. Figure S3

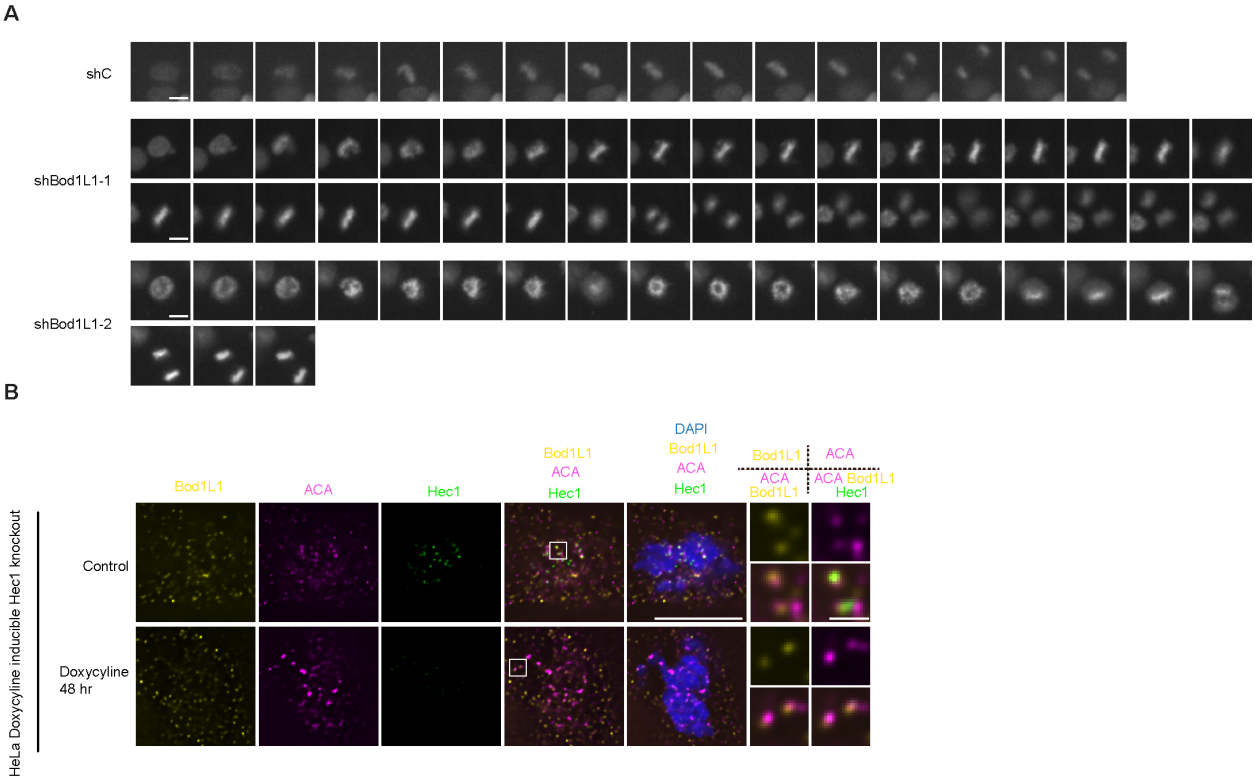

1265

Kucharski et al. Figure 6

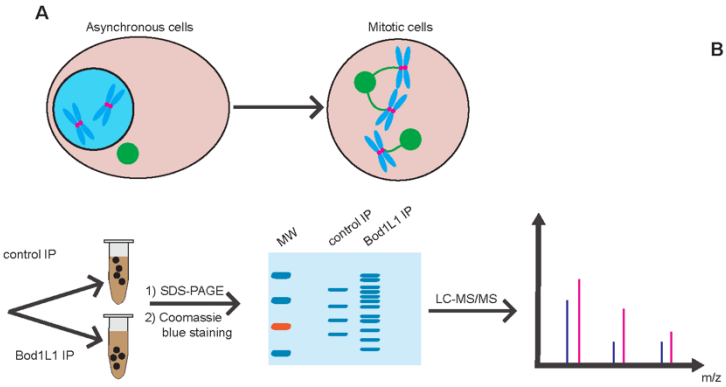

B

Protein ID	Number of peptides in control IP	Number of peptides in Bod1L1 IP
Bod1L1	0	62
Rictor	0	30
PRPF8	0	31
MAPKAP1	0	13
Sgo2	0	4
CENPF	0	6
MCAK	4	8
PP2R1A	2	15
PP2R1B	0	3
PP2CA	1	3
PP2R5E	0	5
Numa	0	5
AurKA	0	2
APC3	0	4
APC8	0	5

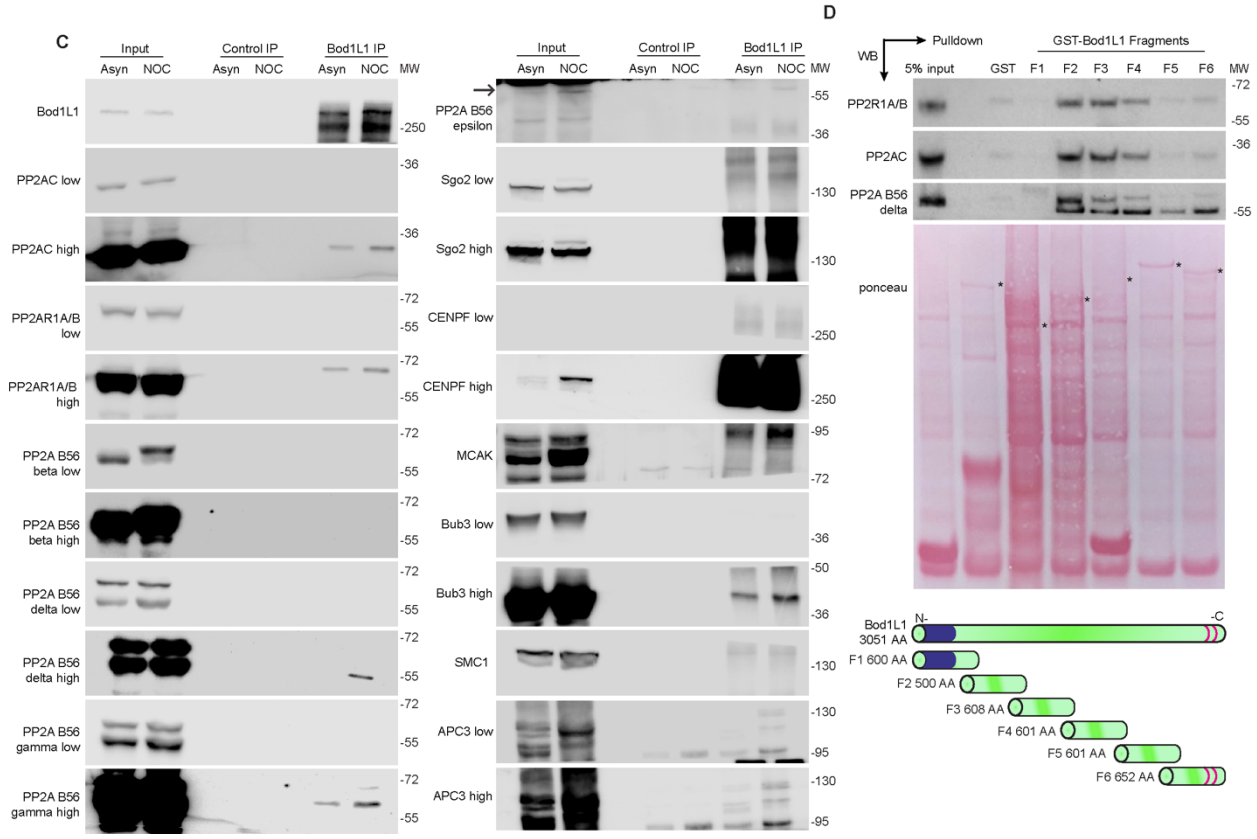

1266

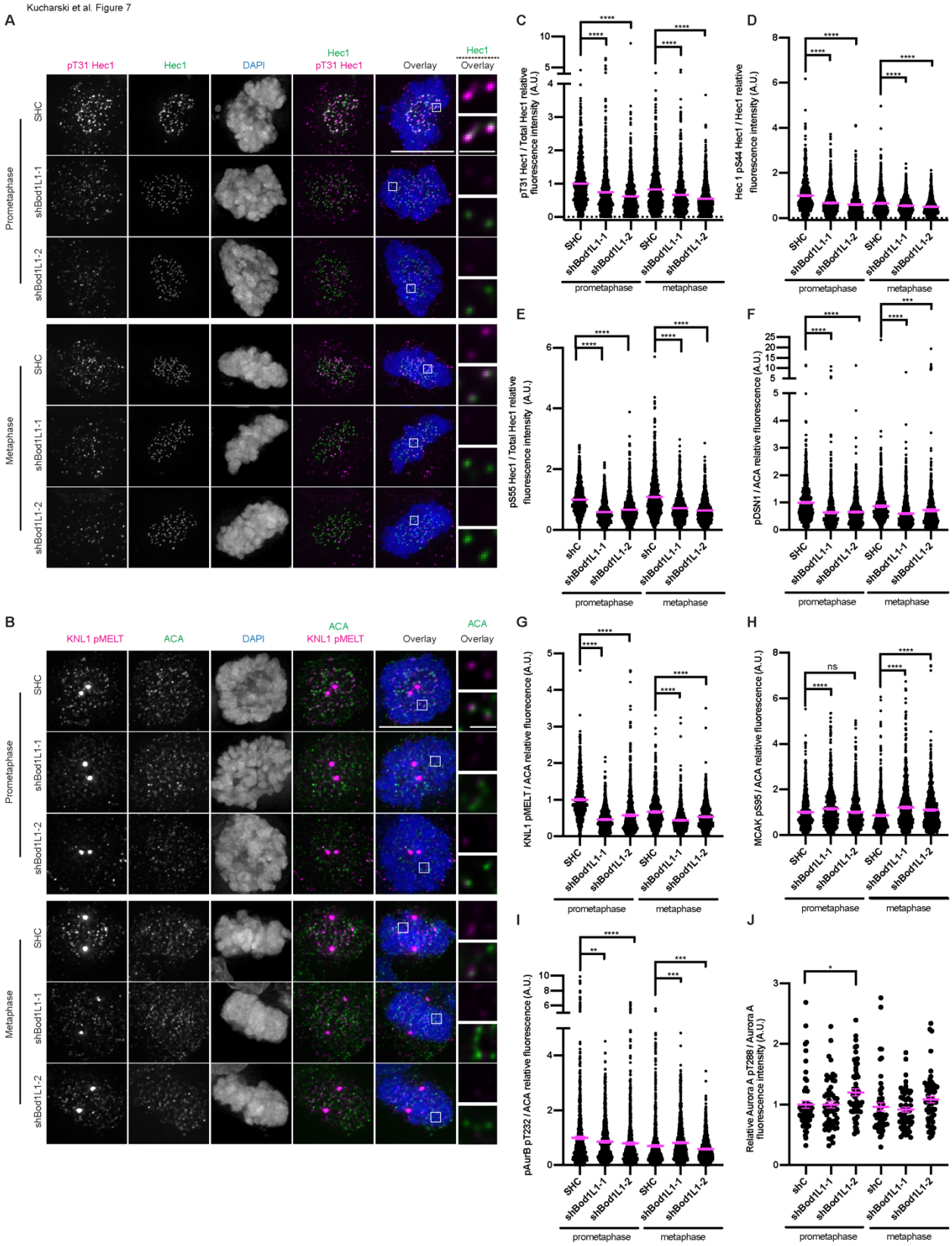
Kucharski et al. Figure 7
A
pT31 Hec1
Hec1
DAPI
Hec1
pT31 Hec1
Overlay
Hec1
Overlay
Prometaphase
Metaphase
SHC
shBod1L1-1
shBod1L1-2
B
KNL1 pMELT
ACA
DAPI
ACA
KNL1 pMELT
Overlay
ACA
Overlay
C
pT31 Hec1 / Total Hec1 relative fluorescence intensity (A.U.)
D
Hec 1 pS44 Hec1 / Hec1 relative fluorescence intensity (A.U.)
E
pS55 Hec1 / Total Hec1 relative fluorescence intensity (A.U.)
F
pDSN1 / ACA relative fluorescence (A.U.)
G
KNL1 pMELT / ACA relative fluorescence (A.U.)
H
MCAK pS95 / ACA relative fluorescence (A.U.)
I
pAurB pT232 / ACA relative fluorescence (A.U.)
J
Relative Aurora A pT288 / Aurora A fluorescence intensity (A.U.)
shC
shBod1L1-1
shBod1L1-2
prometaphase
metaphase
****
***
**
*
ns

Kucharski *et al.* Figure 8

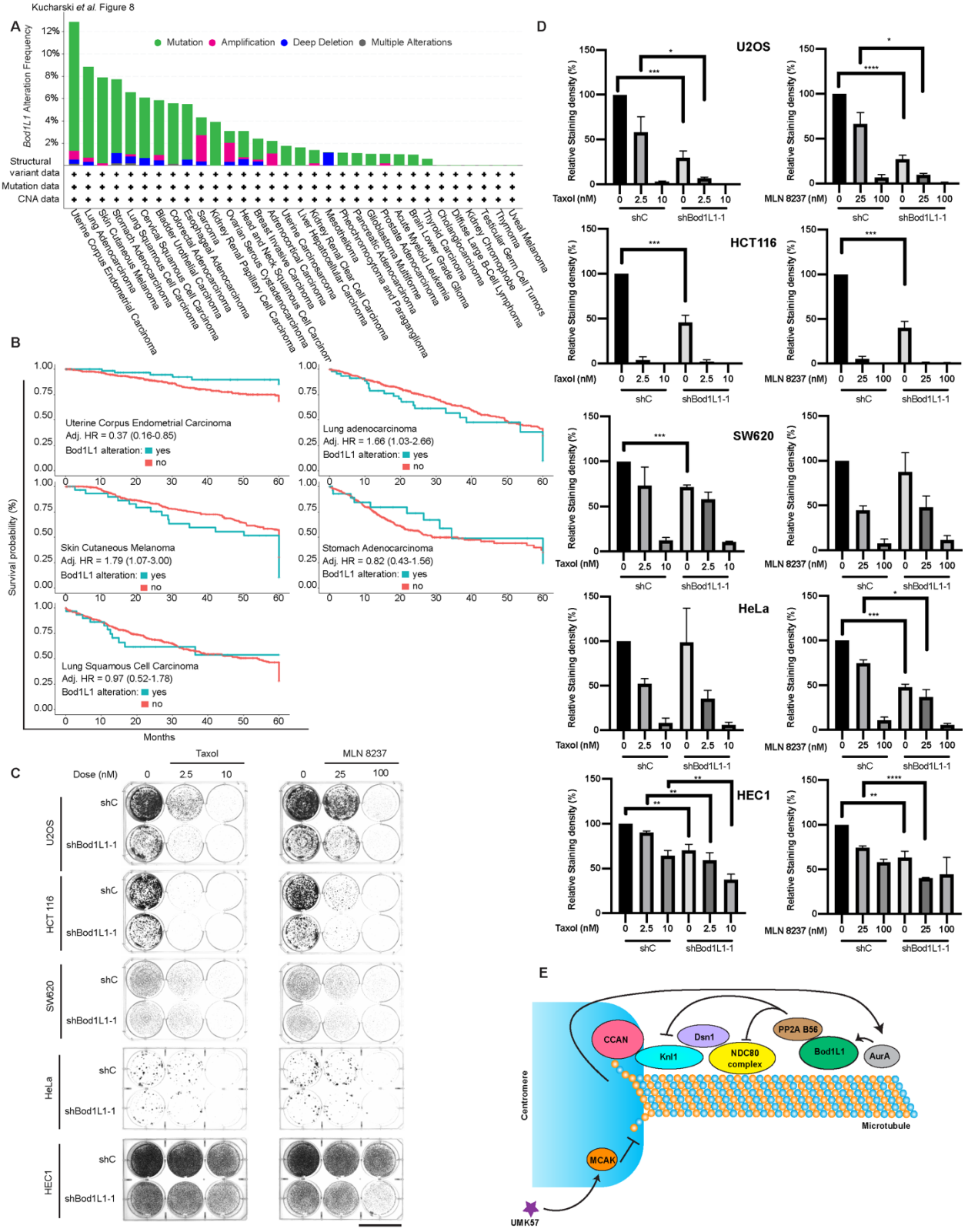

1268

1269

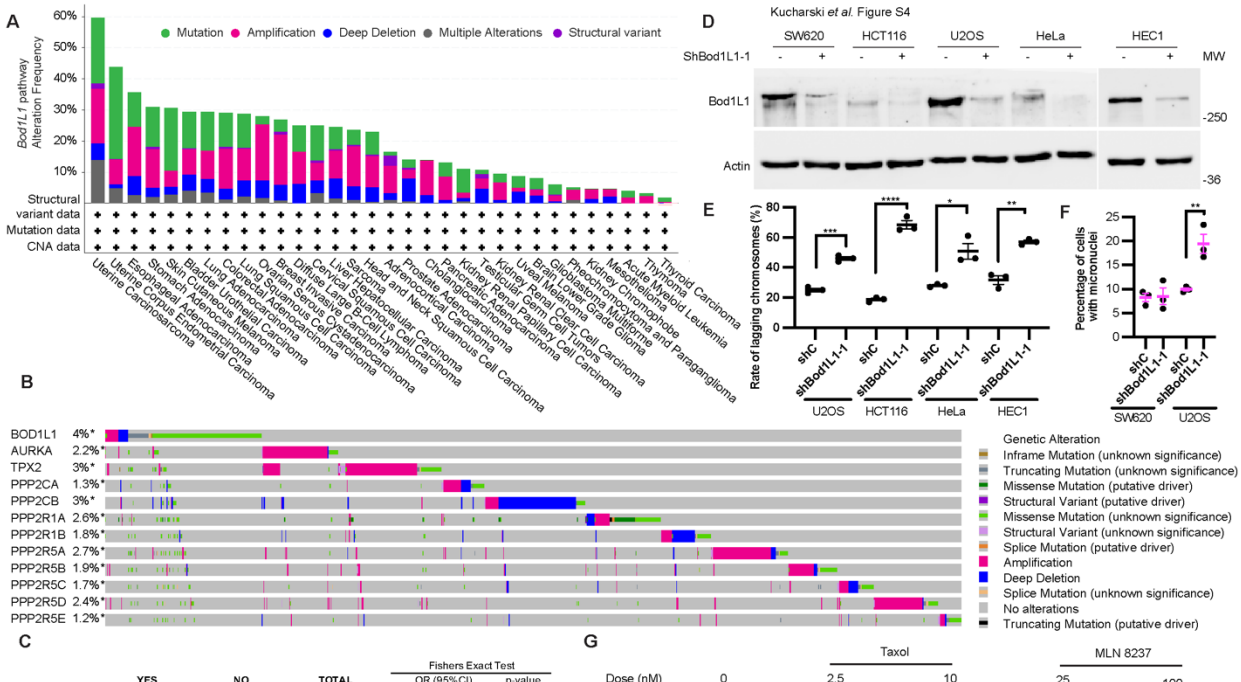

C

	YES	NO	TOTAL	Fishers Exact Test OR (95%CI)	p-value
Any Pathway Gene Altered					
YES	171 (1.56%)	257 (2.34%)	428 (3.9%)	2.99 (2.44-3.67)	1.26E-24
NO	1916 (17.47%)	8623 (78.63%)	10539 (96.1%)		
TOTAL	2087 (19.03%)	8880 (80.97%)	10967 (100%)		
Altered AURKA					
YES	27 (0.25%)	401 (3.66%)	428 (3.9%)	3.32 (2.12-5.05)	5.01E-07
NO	209 (1.91%)	10330 (94.19%)	10539 (96.1%)		
TOTAL	236 (2.1%)	10731 (97.9%)	10967(100%)		
Altered TPX2					
YES	47 (0.43%)	381 (3.47%)	428 (3.9%)	3.78(2.68 -5.24)	1.44E-12
NO	333 (3.04)	10206 (93.06 %)	10539 (96.1%)		
TOTAL	380 (3.47%)	10587 (96.53%)	10967 (100%)		
Altered PPP2CA					
YES	23 (0.21%)	405 (3.69%)	428 (3.9%)	4.89 (2.95-7.78)	7.49E-09
NO	121 (1.10%)	10418 (94.99 %)	10539 (96.1%)		
TOTAL	144 (1.31%)	10823 (98.68%)	10967 (100%)		
Altered PPP2CB					
YES	36 (0.33%)	392 (3.57%)	428 (3.9%)	3.06 (2.07-4.40)	5.66E-08
NO	307 (2.8%)	10232 (93.3%)	10539 (96.1%)		
TOTAL	343 (3.13%)	10624 (96.87%)	10967 (100%)		
Altered PPP2R1A					
YES	39 (0.36%)	389 (3.55%)	428 (3.9%)	4.14 (2.83-5.92)	7.99E-12
NO	249 (2.27%)	10290 (93.83%)	10539 (96.1%)		
TOTAL	288 (2.63%)	10679 (97.38%)	10967 (100%)		
Altered PPP2R1B					
YES	33 (0.30%)	395 (3.60%)	428 (3.9%)	5.09 (3.35-7.55)	2.25E-12
NO	170 (1.55%)	10369 (94.55%)	10539 (96.1%)		
TOTAL	203 (1.85%)	10764 (98.15%)	10967 (100%)		
Altered PPP2R5A					
YES	41 (0.37%)	387 (3.53%)	428 (3.9%)	4.29 (2.96-6.09)	9.45E-13
NO	254 (2.32%)	10285 (93.78%)	10539 (96.1%)		
TOTAL	295 (2.69%)	10672 (97.31%)	10967 (100%)		
Altered PPP2R5B					
YES	31 (0.28%)	397 (3.62%)	428 (3.9%)	4.44 (2.89-6.63)	1.96E-10
NO	182 (1.66%)	10357 (94.44%)	10539 (96.1%)		
TOTAL	213 (1.94%)	10754 (98.06%)	10967 (100%)		
Altered PPP2R5C					
YES	27 (0.25%)	401 (3.66%)	428 (3.9%)	4.54 (2.86-6.96)	1.73E-09
NO	154 (1.40%)	10385 (94.69%)	10539 (96.1%)		
TOTAL	181 (1.65%)	10786 (98.35%)	10967 (100%)		
Altered PPP2R5D					
YES	33 (0.30%)	395 (3.60%)	428 (3.9%)	3.68 (2.44-5.40)	3.77E-09
NO	234 (2.13%)	10305 (93.96%)	10539 (96.1%)		
TOTAL	267 (2.43%)	10700 (97.56%)	10967 (100%)		
Altered PPP2R5E					
YES	24 (0.22%)	404 (3.68%)	428 (3.9%)	5.53 (3.36-8.76)	4.33E-10
NO	112 (1.02%)	10427 (95.08%)	10539 (96.1%)		
TOTAL	136 (1.24%)	10831 (98.76%)	10967 (100%)		
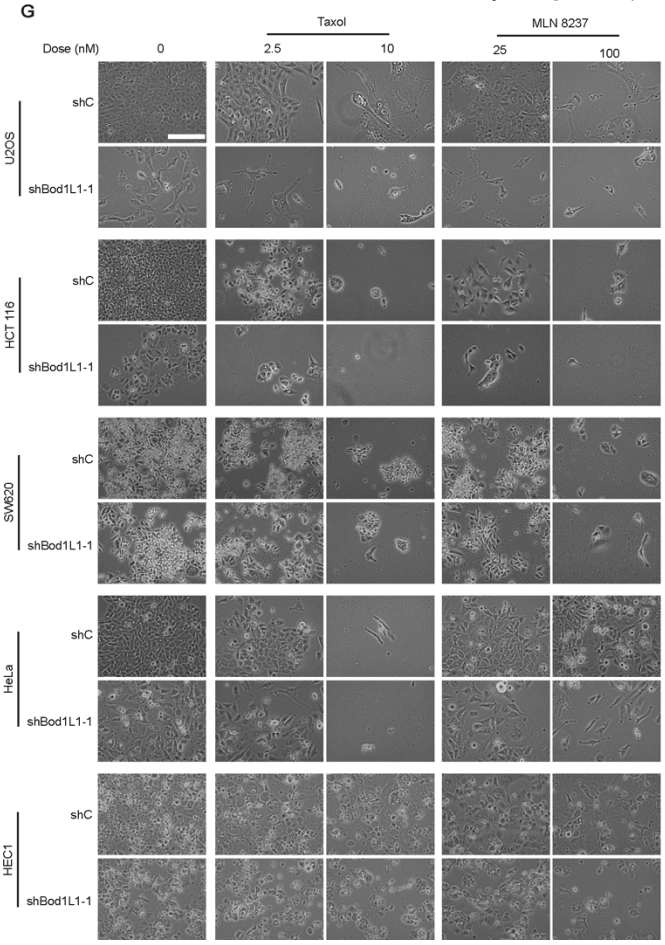
Altered BOD1L1